FLUORESCENT LABELING OF HUMAN EMBRYONIC STEM CELL -DERIVED NEURONS AND CHARACTERIZATION OF THEIR NETWORK CONNECTION DEVELOPMENT

Master's Thesis

Meeri Mäkinen

Institute of Biomedical Technology

University of Tampere

January 2012

Acknowledgements

This study was carried out at NeuroGroup, Institute of Biomedical Technology (IBT), University of Tampere, Finland. I wish to warmly thank our group leader and my supervisor Susanna Narkilahti, PhD, Docent, for believing in my ideas and for allowing me to conduct this journey under her guiding wing of scientific wisdom. I would also wish to acknowledge Riikka Äänismaa, PhD, for enlighting me with her strong knowledge in cell culturing as well as Kim Larsson, PhD, for providing his expertise and assistance in the field on imaging. I also wish to express my gratitude towards my colleague and friend Laura Ylä-Outinen, MSc, for her irreplaceable guidance and for all the electrophysiology conversations. In addition, I am grateful to my colleague and friend Tiina Joki for her opinions, support and for all the delightful walks in the rims of reality. Finally, I wish to present my gratitude to my mother Pirkko who taught me persistence, to my father Antero who taught me inventiveness, to my brother Manu who is always there for me and to Janne for understanding my weird ways.

Because of you, every day is a glorious day for science.

Tampere, January 2012

Meeri Mäkinen

Pro Gradu –tutkielma

Paikka:	TAMPEREEN YLIOPISTO Biolääketieteellisen teknologian yksikkö (IBT)
Tekijä:	MÄKINEN, MEERI EEVA-LIISA
Otsikko:	Ihmisalkion kantasoluista johdettujen hermosolujen fluoresenssileimaaminen ja niiden muodostamien verkkojen yhteyksien muodostuminen
Sivumäärä:	79
Ohjaaja:	Dosentti, FT Susanna Narkilahti
Tarkastajat:	Professori Markku Kulomaa ja Dosentti, FT Susanna Narkilahti
Aika:	Tammikuu 2012

Tiivistelmä

Solusiirrehoidot ovat vaihtoehtoinen hoitomuoto vaikeasti parantuvien ja hoidettavien kudosten, kuten keskushermostokudoksen, vaurioiden korjaamiseen. Solusiirteiden tunnettuja ongelmia ovat kuitenkin siirrettyjen solujen heikko selviytyminen ja kyvyttömyys liittyä toimivaksi osaksi kohdekudosta. On havaittu, että tapa jolla keskushermostoon siirrostetut solut liittyvät osaksi kudosta, muistuttaa tapaa, jolla alkionkehityksen aikana muodostuvat uudet hermosolut liittyvät vasta muodostuvaan keskushermostokudokseen. Tämän alkionkehitysvaiheen aikana hermoverkoissa esiintyy spontaania verkostoaktiivisuutta. Samankaltaista aktiivisuutta esiintyy myös alkion kantasoluista laboratorio-olosuhteissa erilaistetuissa hermoverkoissa. Tämän tutkimuksen tavoitteena oli optimoida alkion kantasoluista erilaistettujen hermosolupopulaatioiden tarkkailuun soveltuvia fluoresenssivärjäysmenetelmiä, sekä selvittää varhaisimpien hermoverkkoyhteyksien muodostumista.

Tutkimuksessa käytetyt hermosolut erilaistettiin laboratoriossa ihmisalkion kantasoluista ja värjättiin fluoresoivilla molekyyleillä (CT, SR101). Värien säilymistä, niiden vaikutusta solujen elinkykyyn ja jakaantumiseen, niiden solutyyppispesifisyyttä, sekä soveltuvuutta yhteisviljelmien tarkkailuun tutkittiin kuvantamisella, elinkykymäärityksillä, immunosytokemialla ja mikroelektrodihilamittauksilla. Varhaisten verkkoyhteyksien ja verkkoaktiivisuuden muodostumista tutkittiin altistamalla solut mikroelektrodihilamittauksen tai kalsiumkuvantamisen aikana eri yhteyksiin vaikuttaville aineille.

CT:llä optimaalisin värjäytyminen saatiin aikaan altistamalla solut 10µM pitoisuudelle 72h ajan. SR101:llä puolestaan riitti 8h altistusaika 10µM pitoisuudessa. CT säilyi soluissa 4 viikon ajan, ei vaikuttanut solujen jakaantumiseen tai elinkykyyn ja värjäsi kaikki solut. CT havaittiin soveltuvaksi yhteisviljelmien värjäykseen. SR101 vaikutti värjäävän astrosyyttejä solulinja- ja kypsyysriippuvaisesti. Varhaisen hermoverkkoaktiivisuuden havaittiin välittyvän aukkoliitosten, glutamatergisten ja GABAergisten yhteyksien välityksellä, täten muistuttaen *in vivo* muodostuneiden verkkojen aktiivisuutta.

Master's Thesis

Place:	UNIVERSITY OF TAMPERE Institute of Biomedical Technology (IBT)
Author:	MÄKINEN, MEERI EEVA-LIISA
Title:	Fluorescent labeling of human embryonic stem cell –derived neurons and characterization of their network connection development
Pages:	79
Supervisor:	Susanna Narkilahti, PhD, Docent
Reviewers:	Professor Markku Kulomaa and Susanna Narkilahti, PhD, Docent
Date:	January 2012

Abstract

Cell transplantation therapy is an alternative treatment for defects in tissues with poor regeneration and lack of efficient treatments. One of such tissues is the central nervous system tissue. However, cell transplantation therapies of the central nervous system are known to suffer from the poor survival and inability of the transplanted cells to integrate as a functional part of the target tissue. The integration of transplanted cells into the central nervous system has been observed to resemble the integration of newborn into the developing brain of the fetus. This developmental period is characterized by spontaneous neural network activity. Similar network activity has been observed to form in embryonic stem cell derived neural networks. The aim of this study was to optimize fluorescence labeling methods to allow the visualization of combined human embryonic stem cell derived neural cell populations and to study the formation of the earliest network connections.

Neural cells were derived from human embryonic stem cells and labeled with fluorescent dyes (CT, SR101) using different concentrations and incubation times. Retainment, effect on cell viability and proliferation, cell type specificity and suitability for co-culturing were studied with imaging, fluorescent staining, immunocytochemistry and microelectrode arrays. The formation of the earliest network connections was studied pharmacologically by measuring the change in activity with either microelectrode arrays or calcium imaging.

The optimal parameters for CT were 72 hour incubation in 10μM dye concentration and for SR101 8 hour incubation in 10μM dye concentration. CT was able to label cells up to a 4 week observation period, did not affect cell proliferation or viability and labeled all the cell types. CT was found to be suitable for co-culturing studies. SR101 seemed to label astrocytes dependent on cell line and maturation stage. The early network activity was found to be mediated by gap junctions, glutamatergic and GABAergic connections, thus resembling the connectivity observed to occur during development.

Abbreviations

AM	Acetoxymethyl
AMPA	2-amino-3-(5-methyl-3-oxo-1,2-oxazol-4-yl)propanoic acid
BDNF	Brain derived neurotrophic factor
Bic	Bicuculline
BSA	Bovine serum albumin
bFGF	Basic fibroblast growth factor
CBX	Carbenoxolone
CFDA	Carboxyfluorescein diacetate
CMFDA	Chloromethyl carboxyfluorescein diacetate
CNS	Central nervous system
CT	CellTracker Green
DAPI	4',6-diamidino-2-phenylindole
DiD	1,1'dioctadecyl-3,3,3',3'-tetramethylindodicarbocyanine perchlorate
DMEM	Dulbecco's modified Eagle's medium
DPBS	Dulbecco's phosphate buffered saline
ESC	Embryonic stem cell
EthD-1	Ethidium homodimer
FDA	Fluorescein diacetate
GABA	Gamma-aminobutyric acid
GFAP	Glial fibrillary acidic protein
GZA	Glycyrrhizic acid
hESC	Human embryonic stem cell
MAP-2	Microtubule-associated protein 2
MCS	MultiChannel Systems
MEA	Microelectrode array
NDS	Normal donkey serum
NMDA	N-methyl-D-aspartate
SR101	Sulforhodamine 101

Table of Contents

1. Introduction

The central nervous system (CNS) can be damaged due to a sudden trauma or a disease. Due to the structural complexity, poor endogenous regeneration capability and lack of efficient treatments, the acquired CNS defects are often permanent. Cell transplantation therapy is a potential alternative form of treatment for recovering permanent tissue defects. Cell transplantation therapies are based on the transplantation of healthy cells into the target tissue to recover the functionality lost due to the death of endogenous cells. Currently, CNS cell transplantation therapies suffer from a poor cell survival and from the inability of the transplanted cells to integrate as a functional part of the neural circuits in the target tissue (Pluchino et al., 2004; Jäderstad et al., 2010).

The abilities of a cell to survive or integrate properly depend on its cell type (Alexander and Bruneau, 2010). Pluripotent stem cells are cells with the potential to differentiate to any of the cell types hosted within the tissues of an individual. Pluripotent stem cells, such as embryonic stem cells (ESCs), can be *in vitro* differentiated to the neural cells (Görtz et al., 2004; Ban et al., 2007; Illes et al., 2007; Heikkilä et al., 2009; Illes et al., 2009; Lappalainen et al., 2010). Thus, pluripotent stem cell derived neurons form a potential source for transplantation therapies of the CNS. However, the ability of the cells to survive and form neural circuits *in vitro* should be studied in great detail in order to gain insight into their suitability for transplantation.

The integration of transplanted cells into CNS has been observed to resemble the integration of newborn neurons into the neural circuits of the developing brain (Jäderstad et al., 2010). During this developmental period the neural circuits exhibit a sequence of spontaneous neural network activity patterns (Dupont et al., 2006). Similar network activity patterns, in turn, have been observed to occur in ESC –derived neural networks *in vitro (*Görtz et al., 2004; Ban et al., 2007; Illes et al., 2007; Heikkilä et al., 2009; Illes et al., 2009; Lappalainen et al., 2010*)*. Hence, ESC-derived neural networks form an ideal environment to study the aspects of integration into functional networks.

2. Review of the literature

2.1. Generation of neural cells from stem cells *in vitro* and *in vivo*

Neural cells have been successfully differentiated from both animal and human embryonic stem cells (ESCs) as well as from induced pluripotent stem cells. Several techniques have been utilized to carry out the differentiation and the most used include embryoid body formation, sphere formation, monolayer cultures and co-cultures (Germain et al., 2010). The embyoid bodies are spherical culture systems containing extra embryonic endoderm surrounding a core, which has the potential to generate cells of all three primary germ layers, ectoderm, mesoderm and endoderm (Germain et al., 2010). The formation of neural ectoderm has been argued to be the default cell fate, which *in vivo* results from the blockage of signals inducing the formation of the other germ layers (Germain et al., 2010).

As the *in vivo* neural ectoderm develops further, it undergoes neurulation to give rise to the neural tube. During this developmental reorganization, the cells of the neural ectoderm, increase their numbers with symmetric divisions and further mature into radial glial cells (Kang et al., 2009). Rosette structures, the culture analogs of the neural tube, have been observed to form during *in vitro* differentiation (Germain et al., 2010). The rosette structures and the neural tube consist of a lumen surrounded by radially organized neural stem cells (Kang et al., 2009; Germain et al., 2010). The neural stem cells of the rosettes resemble the radial glial cells of the developing brain (Germain et al., 2010). In the neural tube, the radial glial cells further divide both symmetrically and asymmetrically to self-renew and generate restricted intermediate progenitor cells and neurons (Kang et al., 2009).

Neural tube formed during the neurulation is patterned into different regions with respect to its closure site (Germain et al., 2010). Similar to the neural tube, the rosette structures also have regional identities and they are suggested to be induced by the local signaling centers formed spontaneously *in vitro* (Germain et al., 2010). An additional similarity between the neural tube and the rosette structure is the ability of the resident cells to respond differently to same signals, depending on their lineage history and fate (Germain et al., 2010).

The developing neural tube contains patterning for the prospective regions of midbrain, hindbrain and spinal cord (Germain et al., 2010). The anterior part of the midbrain region of the neural tube further develops into the forebrain (Germain et al., 2010). As the forebrain develops, it becomes further divided into dorsal and ventral domains (Gaspard et al., 2008; Germain et al., 2010). The neural precursor population generated by the *in vitro* differentiation can be, as well, divided on the basis of the expressed markers, into cell populations of anterior neural ectoderm (midbrain, hindbrain and spinal cord), dorsal forebrain or ventral forebrain identity (Gaspard et al., 2008).

During *in vivo* neurogenesis, the distinct regions of the brain produce different types of neurons. The progenitor cell population of the dorsal forebrain gives rise to projection neurons, while the ventral population gives rise to interneurons and striatal neurons (Gaspard et al., 2008; Germain et al., 2010). Midbrain, on the other hand, gives rise to dopaminergic and hindbrain to serotonergic neurons (Germain et al., 2010). The neural progenitor cells can be identified by the expression of nestin and as the cells progress further along the neural lineage they begin the expression of neuronal markers beta-tubulin-III and microtubule-associated protein 2 (MAP-2) (Gaspard et al., 2008).

The projection neurons of the cerebral cortex are generated by a sequential neurogenesis (Germain et al., 2010). During the sequential neurogenesis, different types of neurons are generated sequentially and they will populate different cortical layers (Gaspard et al., 2008). Cortical layers are formed as the sequentially generated neurons move to their final locations (Germain et al., 2010). The earliest generated neurons form the innermost layers while the neurons born later migrate across the newborn inner layers to form more external layers (Germain et al., 2010).

During the progression of the sequential neurogenesis, the neural precursor cell competency changes accordingly (Gaspard et al., 2008). Similar to this *in vivo* phenomenon, the neural stem cells differentiated from pluripotent stem cells also show the ability to change their differentiation potential during a sequential neurogenesis (Germain et al., 2010). Furthermore, there is evidence that the neurons differentiated as adherent cultures can organize into laminar structures which bear resemblance to the cortical layers (Germain et al., 2010).

Soon after their generations, the newborn neurons begin to migrate to their respective layers. After the neurons have arrived at their target layer, they undergo a final maturation step, during which they develop selective patterns of gene expression and connections

(Gaspard et al., 2008). Similarly in cultures, post-migratory cells start to participate in the synchronous network activity and become integrated into the network (de Lima et al., 2008).

After neurogenesis, the remaining radial glial stem cells differentiate into glial fibrillary acidic protein (GFAP) expressing cells, astroglial precursors and finally to astrocytes (Gaspard et al., 2008; Germain et al., 2010). Similarly to *in vivo* progenitors, it has been observed that the *in vitro* differentiated neural stem cells change their potency towards glial cell and astrocyte production (Germain et al., 2010).

2.2. Electrical properties of single cells and networks

Electrically active cells, such as neurons, are able to produce current flows across their plasma membrane. These current flows are produced by the ions moving through the ion channels of the cell membrane. Different types of ion channels can be opened by different mechanisms, ligand binding or membrane potential change. The kinetics of ion channels affects the kinetics of the currents flowing through a certain population of ion channels. As these ion movements are able to change the cell membrane potential they also determine the kinetics of membrane potential changes. In addition, as ions exit and enter the cell via ion channels, current sinks and sources are generated outside the cell due to the local changes in ion concentrations (Claverol-Tinture and Pine, 2002; Morin et al., 2005). An electrical potential difference, known as the extracellular field potential, is formed between these sinks and sources (Claverol-Tinture and Pine, 2002; Morin et al., 2005).

It is generally believed, that neuronal action potentials cause the very fast extracellular field potential changes, while the slow changes are caused by other ion channel based membrane phenomena, such as simultaneous post synaptic currents of several neurons (Claverol-Tinture and Pine, 2002; Morin et al., 2005).

The electrical properties and activity of neurons are generally studied with methods which measure changes in the ion concentrations. Electrodes can be used to measure the electrical potential changes arising from the changes in ion concentrations inside or outside the cell. Another common approach is to use ion or voltage sensitive dyes which generate a fluorescence signal upon binding to an ion or upon a membrane potential change.

2.3. Extracellular electrical properties of groups of electrically active cells

In neural cell culture or in living nervous tissue, the extracellular field potentials interact as adjacent cells produce adjacent current sinks and sources. The interaction between adjacent sinks and sources can be constructive or destructive and the result is a local field potential (Morin et al., 2005). The local field potential describes the electrical activity within a volume of a culture or a tissue (Morin et al., 2005) and contains a collection of fast action potentials superimposed on a slow-varying potential arising from other electrical phenomena (Rochefort et al., 2009; Gullo et al., 2010).

The local field potentials of neural culture or tissue can be measured with extracellular electrodes. The two components, action potentials and other currents, of the recorded local field potential are generally separated by filtering and only one of them is studied in more detail. Multiunit activity contains only the high frequency components (with frequency of 200-6000Hz) of the extracellular local field potential signal and is thought to represent the actual spiking of nearby neurons (Burns et al., 2010; Mattia et al., 2010). The filtered local field potential, on the other hand, is gained by filtering out the higher frequency components (individual spike components, 200Hz) and is thought to reflect the synaptic input to a neuron population (Burns et al., 2010; Gullo et al., 2010; Mattia et al., 2010). The exact relationship between the filtered local field potential and multiunit activity, however, seems to be unclear (Burns et al., 2010).

2.3.1. The effect of extracellular environment on the electrical properties of cells

The extracellular solution is known to have an effect on the electrical properties of neurons. The resting membrane potential is formed by the voltage difference between the extra- and intracellular fluids across the cell membrane. The ionic composition of the surrounding extracellular environment is known to influence the resting membrane potential according to Goldman-Hodgkin-Katz equation. Goldman-Hodgkin-Katz equation describes how the membrane potential is formed by the differences in ion concentrations across the membrane. By generating a deviation from the physiological ion concentrations of the extracellular fluids, for example with high K^+ concentration, the neural cell membrane potential can be changed and even depolarized enough to produce action potentials. In addition, on a single cell level, the action potential firing threshold is affected by extracellular divalent cations such as Ca^{2+} and Mg^{2+}. Ca^{2+} and Mg^{2+} cations are known

to reduce the excitability of the neurons by raising the action potential firing threshold (Canepari et al., 1997).

2.3.2. The influence of extracellular solution ion composition on networks

In addition to the membrane properties of the constituent neurons, the synaptic signaling in a network of neurons can be affected by the concentrations of extracellular ions as the changes in the electrical properties of single neurons can give rise to changes in the whole network. For example, if the constituent neurons are slightly depolarized with higher extracellular K^+ the whole network becomes more excitable and active (Sun and Luhmann, 2007).

The effect on network activity can also be mediated by changes in the communication between the constituent neurons. The extracellular Ca^{2+} ions affect the synaptic signaling by affecting synaptic currents. A low Ca^{2+} ion concentration depresses the synaptic currents while a high concentration will enhance the synaptic currents. These effects arise from the role of Ca^{2+} ion flow in triggering the release of synaptic transmitter vesicles. Mg^{2+} is also able to affect the presynaptic terminal. Mg^{2+} ions act on the presynaptic terminal by inhibiting transmitter release. In addition, Mg^{2+} ions can act postsynaptically by blocking glutamate receptors. (Canepari et al., 1997)

Because the ionic concentrations in the extracellular environment affect the activity of single neurons and their networks, it is an important aspect to consider when designing studies assessing the electrical properties of single neurons or neural networks.

2.4. Spontaneous network activity in stem cell derived neural cultures

2.4.1. Development of electrophysiological properties of single cells

The development of single cell level activity of neurons differentiated from ESCs has been previously followed by performing intracellular electrode measurements (Ban et al., 2007). The intracellular electrode measurements are also known as patch clamp measurements. By using this methodology the *in vitro* differentiated neurons have been shown to be able to fire single and repetitive action potentials as response to injected currents similar to *in vivo* differentiated neurons (Ban et al., 2007; Illes et al., 2009).

2.4.2. Development of the electrical network activity

A period of synchronized network activity occurs in a maturing network simultaneously with a period of synapse formation and elimination both *in vivo* and *in vitro* (Chiappalone et al., 2006). Microelectrode array (MEA) measurements and calcium imaging have been utilized to describe stages of spontaneous activity pattern generation during the development of activity in primary cell derived neural networks (O'Donovan, 1999; Chiappalone et al., 2006). The first form of network activity in primary cultures is generated before the formation of chemical synaptic networks and it is formed by coordinated calcium transients between coupled cell groups (O'Donovan, 1999). As the neural network matures, the chemical synapses become the main signal mediating mechanism and the network wide synchronous activity becomes abolishable by voltage gated Na^{2+} channel blockers and chemical synaptic transmitter antagonists (O'Donovan, 1999).

Functional neuronal networks have also been derived *in vitro* from pluripotent stem cells. The formation of a functional network has been shown for neurons differentiated from variable stem cells, such as human and mouse embryonic stem cells (Ban et al., 2007; , Illes et al., 2007; Heikkilä et al., 2009; Illes et al., 2009; Lappalainen et al., 2010) or human teratocarcinoma cells (Görtz et al., 2004).

2.4.3. Phases of neural network development in stem cell derived networks

The development of stem cell derived neuronal networks can be divided into distinct phases based on the nature of the observed network activity. This pattern of phases is generally followed regardless of the efficacy of neuronal derivation (Lappalainen et al., 2010), species (Görtz et al., 2004; Ban et al., 2007; Illes et al., 2007; Heikkilä et al., 2009; Illes et al., 2009; Lappalainen et al., 2010), or the differentiation protocol itself (Görtz et al., 2004; Ban et al., 2007; Illes et al., 2007; Heikkilä et al., 2009; Illes et al., 2009; Lappalainen et al., 2010). Thus, it could be argued that this is an intrinsic pattern of activity for occurring in all properly developing neural networks. The described stages advance from a single spiking phase to a final phase of spatially distributed synchronous oscillating bursts (Illes et al., 2007).

The first phase of the network activity maturation in *in vitro* networks is the appearance of uncorrelated and randomly distributed extracellular voltage signals representing single spikes (Görtz et al., 2004; Ban et al., 2007; Illes et al., 2007, Heikkilä et al., 2009; Lappalainen et al., 2010). This random single spiking activity seems to appear

independent of whether the cells are differentiated as aggregates or monolayers (Illes et al., 2009). The appearance of single spikes is also independent of the length of the differentiation period (Lappalainen et al., 2010). In teratocarcinoma derived neural cultures, the single spiking has been reported as the only form of network activity observed during more than 12 weeks period (Görtz et al., 2004) indicating the inability of these networks to reach functionally more mature stages.

The second phase of network activity maturation is the occurrence of spike trains. The definition of a spike train varies from publication to another, but in stem cell derived networks it has been described to consist of 3 to 7 spikes within 300ms (Illes et al., 2007) or more stringently as more than 5 spikes with a regular inter-spike interval of 20-100ms (Heikkilä et al., 2009). The occurrence spike trains have been observed in both neural aggregate and monolayer cultures as well as in human and mouse ESC-derived networks (Illes et al., 2007; Heikkilä et al., 2009; Illes et al., 2009).

The third phase of the maturation of the neural network activity is the occurrence of synchronous bursting of several neurons detected on a single or on several electrodes. The bursts can be generally described as very dense spike trains. However, the exact definition varies between publications. The third phase has been observed to appear in mouse and human ESC-derived neural aggregate cultures (Ban et al., 2007; Illes et al., 2007; Heikkilä et al., 2009; Illes et al., 2009). However, the aggregate cultures do not always develop synchronous bursting spontaneously and without pharmacological intervention (Illes et al., 2009) while the networks differentiated as monolayer cultures have not been observed to mature to this stage at all (Illes et al., 2009).

The bursting patterns also undergo different developmental phases. At first, the bursting is seen on one or few electrodes, but as the network matures further, the bursts appear as synchronous events between several adjacent electrodes (Heikkilä et al., 2009; Lappalainen et al., 2010) and later over most of the electrodes covering a large proportion of the network (Heikkilä et al., 2009). In addition to the synchrony of burst events, the form of bursts has been described to develop from an initial constant mode with similar spike amplitudes to a bell shaped mode of first increasing spike amplitude phase followed by a decreasing spike amplitude phase (Illes et al., 2007; Heikkilä et al., 2009).

Unlike the development of activity in the primary neuronal cultures (O'Donovan, 1999; Chiappalone et al., 2006), the ESC -derived neuronal networks have rarely been reported

to generate periodic bursting separated by clear periods of quiescence (Ban et al., 2007; Illes et al., 2007; Heikkilä et al., 2009).

2.4.4. Conclusions from the spontaneous activity of stem cell derived neural networks

The observations from the developing stem cell derived aggregate (Illes et al., 2007; Heikkilä et al., 2009; Illes et al., 2009; Lappalainen et al., 2010) and monolayer (Görtz et al., 2004; Illes et al., 2009) derived cultures of neural networks suggests that the heterogeneous neural cell population of aggregates is needed to produce a neural network with activity development profile similar to that of primary networks. Interestingly, if neural differentiation is performed as a monolayer this developmental profile is not observed (Ban et al., 2007).

2.5. Mechanisms participating in the generation of early network activity of *in vivo* differentiated neurons

The first form of network activity, synchronized oscillations, in the developing brain is generated by a gap-junction coupled subplate circuits (Khazipov and Luhmann, 2006). The subplate neurons are the first functionally mature neurons of the developing brain and are generated in the beginning of the neurogenesis (Kanold and Luhmann, 2010). Subplate neurons are locally connected to each other and other cortical neurons via gap junctions (Dupont et al., 2006; Kanold and Luhmann, 2010). However, they also form more distant connections via chemical synapses (Kanold and Luhmann, 2010).

During the postnatal development, the cortical network switches from the subplate driven gap junction coupled syncytium to a chemically mediated synaptic network and the subplate is no longer needed (Dupont et al., 2006; Khazipov and Luhmann, 2006). The change in the mediating mechanism is concurrent with changes in the form of the synchronous activity within these networks (Allene and Cossart, 2010). The functions of various synaptic systems has been shown to be required for the normal development of neuronal connectivity, as well as, for the generation of the normal electrical activity patterns (Hogberg et al., 2011) and are briefly described below.

2.5.1. Gap junctions

Gap junctions, also known as the electrical synapses, are intercellular channels which allow small molecules to transfer from one cell to another, thus enabling the biochemical communication between the gap junction coupled cells (Yuste et al., 1995; Kandler, 1998; Khazipov and Luhmann, 2006; Peinado, 2011). The gap junctional complexes between

cells are formed by two connected connexons, each provided by one cell. The connexons, in turn, consist of cell membrane spanning proteins of the connexin family (Yuste et al., 1995; Kandler, 1998; Khazipov and Luhmann, 2006; Peinado, 2011).

The developing cortex has a high gap junction content during the early postnatal period when the network connections are formed (Peinado, 2011). In addition, a functional gap junctional coupling between neurons has been shown to exist during this period (Peinado, 2011). Furthermore, during the postnatal development, neuronal gap junctional coupling decreases sharply and the short radius clusters of coupled neuron disappear leaving nonexistent coupling with the exception of inhibitory neurons (Peinado, 2011).

During the early postnatal development, gap junctions couple neurons into small synchronously active groups (Yuste et al., 1995; Kandler, 1998; Khazipov and Luhmann, 2006; Peinado, 2011). The activation of cells within these cell groups, called neuronal domains, is thought to take place via biochemical signals spreading through gap junctions (Yuste et al., 1995; Kandler, 1998; Peinado, 2011). The secondary messenger inositol-triphosphate has been suggested to be the mediating signaling molecule (O'Donovan, 1999).

The early forms of the synchronous network activity of the developing networks have been shown to become blocked by the gap junction blockers and are hence thought to be mediated by gap junctions (Rouach et al., 2003; Dupont et al., 2006; Sun and Luhmann, 2007; Sun et al., 2008; Takayama et al., 2009; Yang et al., 2009; Peinado, 2011). In addition, gap junction knockout mice show deviance in the appearance of oscillatory network activities (Rouach et al., 2003). However, gap junction blockers seem to be unable to block the very early non-synchronous activity (Sun and Luhmann, 2007) and do not abolish the ability of single neurons to produce intracellular calcium concentration elevations associated with neural activity (Peinado, 2011). As the network activity switches from gap junction coupling towards synaptic transmission, the role of gap junctions becomes less critical and the more mature network activities are not as strongly affected by gap junction blockers (Dupont et al., 2006).

Carbenoxolone (CBX), a widely used gap junction blocker, is a derivative of glycyrrhizic acid (GZA) (Rouach et al., 2003). Unlike CBX, GZA is unable to block gap junctions (Rouach et al., 2003). CBX, but not GZA, has been observed to reversibly inhibit spontaneous, as well as bicuculline induced network activity, by reducing the spiking frequency (Rouach et al., 2003). CBX has also been shown to reduce the neuronal

excitability as high (100μM) concentrations, but similar effect has not been observed in lower (20μM) concentrations (Rouach et al., 2003). GZA and its derivatives, such as CBX, are known to have unspecific effects which are caused by the inhibition of Na^+-K^+ ATPase (Rouach et al., 2003). Thus, CBX seems to be able to specifically block gap junctions in low concentrations and its possible unspecific effects should be similar to those produced by GZA.

2.5.2. Gamma-aminobutyric acid

Gamma-aminobutyric acid (GABA) is a neurotransmitter which, in mature animals, is produced by the inhibitory interneurons of the central nervous system (Baltz et al., 2010). $GABA_A$ receptors are Cl^- permeable channels and in mature neurons cause the inhibitory hyperpolarization of the cell membrane by allowing Cl^- ions to flow into the cell (Baltz et al., 2010).

In young neurons GABA is an excitatory neurotransmitter. The excitatory effect is thought to arise due to the high intracellular Cl^- concentration in young neurons (Baltz et al., 2010). The high intracellular Cl^- concentration leads to the flow of Cl^- ions out of the cell down to their electrochemical gradient (Baltz et al., 2010). The flow of negative charge out of the cell causes a membrane depolarization, thus exciting the cell instead of inhibition.

The high intracellular Cl^- concentration in young neurons occurs due to the expression of the ion co-transportter NKCCl and due to the lack of KCC_2 co-transporter (Baltz et al., 2010). NKCCl co-transportter transfers Cl^- into the cell while KCC_2 co-transportter transfers Cl^- out of the cell (Baltz et al., 2010). During the maturation of neurons, the expression of NKCCl cotransporter decreases while that of KCC_2 increases (Baltz et al., 2010). This transporter population change causes the intracellular Cl^- concentration to become lower than the extracellular Cl^- concentration reversing the direction of Cl^- flow through the ion channels associated with GABAergic receptors (Baltz et al., 2010). The reversion of the electrochemical gradient of Cl^- switches the effect of the neurotransmitter GABA from excitatory to inhibitory (Baltz et al., 2010).

Similar to this *in vivo* phenomenon, the cultured immature primary neurons also depolarize and produce calcium transients as a response to GABA agonist addition (Baltz et al., 2010; Kanold and Luhmann, 2010). These cultured neurons have also been shown to be able to undergo GABA switch during their maturation (Baltz et al., 2010).

Several developmental network oscillation patterns are suggested to depend on the GABAergic signaling (Allene and Cossart, 2010; Baltz et al., 2010). The shift in neurotransmitter GABA action from excitatory to inhibitory occurs concurrently with changes of the network activity development (Baltz et al., 2010). However, a more detailed action of GABA in the developing networks seems to be less clear.

It has been described that during the late fetal stage (E14-E17, in rodents), as the GABAergic neurons integrate to the pre-existing neural network, the activity of the network becomes synchronized (de Lima et al., 2008). The primary cultures of cortical cells from this developmental stage show excitatory GABA dependent calcium transients (Voigt et al., 2001). On the other hand, in a different study, GABA was observed to inhibit the network activity of networks derived from the similar cell source (Kamioka et al., 1996).

The discrepancy observed between cultures from similar sources could be related to the development and changes of the network connections during *in vitro* maturation of the network. A change in the role of the neurotransmitter GABA as a network activity mediating mechanism has been described to occur during the *in vitro* development of primary cultures from late fetal cortical sources (Baltz et al., 2010). When the development of the network activity was followed, it was observed that networks first developed a synchronous periodic bursting pattern which was independent of GABAergic signaling (Baltz et al., 2010). As these *in vitro* networks matured further, an inhibitory GABA signaling dependent temporal clustering and decrease of synchronous activity was observed to take place (Baltz et al., 2010). Networks without GABAergic signaling, on the other hand, continue to express the periodic activity, which finally evolved into an oscillatory bursting (Baltz et al., 2010). However, the GABAergic subplate neurons have been argued to be required for the generation of synchronous oscillatory network activity (Kanold and Luhmann, 2010).

In *in vitro* networks containing inhibitory GABAergic signaling, the competitive $GABA_A$ receptor blocker bicuculline disturbs the mature complex bursting generated by inhibitory GABAergic signaling and the network activity changes into regular bursting characteristic to an earlier phase in the network activity development (Baltz et al., 2010). Bicuculline has also been observed to increase the frequency of network activity (Colonnese and Khazipov, 2010), to increase action potential bursts in single cells (Rouach et al., 2003) and to cause oscillating intracellular calcium concentration rises (Kato-Negishi et al., 2003; Rouach et al., 2003).

2.5.3. Glutamate

Glutamate is a neurotransmitter produced by the excitatory neurons of the CNS. Glutamate is used in signal transduction both synaptically and extrasynaptically. The most common glutamate receptors are the N-methyl-D-aspartate (NMDA), 2-amino-3-(5-methyl-3-oxo-1,2-oxazol-4-yl)propanoic acid (AMPA) and kainate receptors.

As the immature neuronal circuits mature, they incorporate glutamatergic NMDA receptors and begin the switch from subplate driven gap-junction mediated signal transduction to glutamaergic circuits (Khazipov and Luhmann, 2006). Several oscillatory network activities appearing during the maturation of neural networks have been described to be dependent on the glutamatergic signaling (Dupont et al., 2006; Khazipov and Luhmann, 2006; Allène et al., 2008; Yang et al., 2009; Allène and Cossart, 2010; Peinado, 2011).

The network activity in the primary cultures of fetal (E16-E17) cortical cells is inhibited by glutamate agonists (Kamioka et al., 1996) and glutamatergic signaling seems to be the mediating mechanism in the activity events of these networks. Furthermore, the network activities observed in fetal cortical cell primary cultures are glutamate dependent both before and after the switch in the effect of neurotransmitter GABA (Baltz et al., 2010).

2.6. Visualizing cell cultures

Fluorescent dyes can be used to visualize live cells without the need for genetic modification. Dyes synthesized for labeling living cells can be designed to allow long term retention and to be biologically inert and nontoxic. However, fluorescent dyes usually lack the specificity of genetically encoded fluorescent proteins and antibody-antigen recognition obtained by immunostaining of fixed cells.

2.6.1. Membrane tracers

Several fluorescent tracers have been developed for the labeling of the cell plasma membranes. These dyes can be fluorescent tagged analogs of natural lipids, such as phospholipids, sphingolipids, fatty acids, triglycerides, steroids, or lipophilic organic dyes, such as long-chain carbocyanines, aminostyryls and rhodamines (Molecular Probes® Handbook, Section 14.4). The lipophilic nature is required for the insertion into the cell membrane. The membrane tracers generally label the whole cell membrane via lateral diffusion from the site of application and they are rarely transferred between two intact membranes (Molecular Probes® Handbook, Section 14.4). Due to the ability to spread across the cell plasma membrane from a local site of application, the lipophilic dyes are

widely used in neuroanatomical tracing (Molecular Probes® Handbook, Section 14.4). The membrane tracers can be loaded onto the cell membrane directly from dye crystals or via aqueous solution (Molecular Probes® Handbook, Section 14.4).

2.6.2. Membrane impermeant cytoplasmic tracers

Hydrophilic water-soluble dyes are also used in visualizing live cells (Molecular Probes® Handbook, Section 14.3). Due to their hydrophilic nature, these dyes are unable to cross the cell membrane (Molecular Probes® Handbook, Section 14.3). Hydrophilic dyes can be loaded via electroporation, microinjection, pinocytosis or by temporarily permeabilizing the cell plasma membrane (Molecular Probes® Handbook, Section 14.3).

Hydrophilic fluorescent dyes can also enter the cells via active uptake mechanisms. Sulforhodamine 101 (SR101) is a low molecular weight fluorescent hydrophilic sulfonic acid tracer which specifically labels astrocytes *in vivo* and *in vitro* (Nimmerjahn et al., 2004; Kafitz et al., 2008; Molecular Probes® Handbook, Section 14.3). SR101 enters the astrocytes via an unknown transporter system (Nimmerjahn et al., 2004). However, SR101 has also been shown to be taken up by actively firing neurons through endocytic recycling of synaptic vesicles (Molecular Probes® Handbook, Section 14.3). SR101 is known to be able to spread between cells via gap junctions (Nimmerjahn et al., 2004). Furthermore, SR101 has been described to have a developmental profile with increasing percentage of cells with glial morphology labeled along the proceeding postnatal development (Kafitz et al., 2008) suggesting that the uptake mechanism could be appearing as astrocytes mature.

2.6.3. Membrane impermeant nuclear tracers

Membrane impermeant nuclear tracers can be used to study the integrity of the cell membrane. These hydrophilic molecules are unable to cross the intact plasma membrane, but upon membrane damage they gain access to the cell interior where their labeling target is located. The nuclear tracer selectivity is generally based on the binding to the double stranded DNA. (Molecular Probes® Handbook, Section 8.1)

Membrane impermeant ethidium dye, ethidium homodimer (EthD-1), is a highly charged molecule with high affinity for DNA (Molecular Probes® Handbook, Section 8.1). EthD-1 is fluorescent without DNA binding but the binding to DNA causes a 40-fold increase in fluorescence of the dye (Molecular Probes® Handbook, Section 8.1). EthD-1 is commonly used to label the nucleus of dead cells (Molecular Probes® Handbook, Section 8.1).

2.6.4. Membrane permeant cytoplasmic tracers

Membrane permeant cytoplasmic tracers are a group of fluorescent dyes which are initially nonpolar but become polar upon interaction with intracellular molecules. The initial hydrophobic nature allows free diffusion through the cell plasma membrane. The exposure and modification by intracellular enzymes and molecules, on the other hand, allows the dyes to be retained in cells. The retainment is based on the polar nature generated by cleavages due to intracellular enzymes or covalent attachment to intracellular molecules.

The acetoxymethyl (AM) ester forms of several polar fluorescent dyes have been synthesized. The AM moieties mask the charges of polar dyes and thus the AM ester derivatives can be loaded into cells via passive diffusion through the plasma membrane (Molecular Probes® Handbook, Section 14.2). The AM ester forms of fluorescent dyes are generally nonfluorescent until cleavage by intracellular esterases (Molecular Probes® Handbook, Section 14.2). After the cleavage of the AM group, the molecules obtain their previous fluorescent and hydrophilic properties (Molecular Probes® Handbook, Section 14.2). The reappearance of polarity causes the fluorescent molecules to become membrane impermeant and thus they are retained within cells. The cell-permeant fluorescent dyes, including acetoxymethyl esters of calcein, are known to suffer from poor retainment and are retained in living cells only for few hours (Molecular Probes® Handbook, Section 14.2). The cell-permeant esterase derivatives are generally used as viability probes of enzymatic activity (activation of fluorescence) and membrane integrity (intracellular retention of the fluorescent products).

Similar to AM esters, the chloromethyl derivatives of polar dyes are hydrophobic and can passively diffuse through the cell plasma membrane (Molecular Probes® Handbook, Section 14.2). The chloromethyl derivatives are mildly thiol-reactive and within cells undergo a glutathione S-transferase reaction producing complexes with intracellular glutathione sources (Molecular Probes® Handbook, Section 14.2). However, chrolomethyl derivatives of fluorescent tracers have also been suggested to react with other intracellular moieties (Molecular Probes® Handbook, Section 14.2). Due to their attachment to the intracellular macromolecules the chloromethyl derivatives of fluorescent dyes can be retained during immunocytochemistry (Molecular Probes® Handbook, Section 14.2).

Fluorescein diacetate (FDA) is a membrane permeant fluorescent probe which, after entering the cell cytoplasm, can be hydrolyced by intracellular hydrolysis to a fluorescent product, fluorescein (Molecular Probes® Handbook, Section 14.2). The fluorescein,

however, is only briefly retained by the cell plasma membrane (Molecular Probes® Handbook, Section 14.2). The FDA body has been modified to produce a group of FDA derivatives with improved intracellular retainment.

Carboxyfluorescein diacetate (CFDA) is a carboxylic acid derivative of FDA. Similarly to FDA, CFDA undergoes intracellular hydrolysis, however, the resulting molecule, carboxyfluorescein, contains more negative charge compared to fluorescein and is hence retained better (Molecular Probes® Handbook, Section 14.2). Sulfofluorescein diacetate, a sulfonic acid derivative of FDA is similar to CFDA, except the fluorescein sulfonic acid produced by the intracellular cleavage is even more polar than the fluorescein carboxylic acid, thus allowing even better retention (Molecular Probes® Handbook, Section 14.2). These FDA derivatives have stronger polarity than FDA and their AM ester derivatives can be used to produce better membrane permeability caused by the neutralization of the charges produced by carboxyl or sulfonic acid addition (Molecular Probes® Handbook, Section 14.2).

Furthermore, a chloromethyl conjugate of FDA (CMFDA) has been synthesized. CMFDA is a membrane permeable molecule and once inside the cell, the chromethyl moieties react with intracellular thiols and the acetate groups undergo hydrolysis (Molecular Probes® Handbook, Section 14.2). The final product is a fluorescent fluorescein conjugated to an intracellular thiol donor molecule (Molecular Probes® Handbook, Section 14.2). Because chloromethyls react with glutathiones and proteins, some CMFDA can be retained in cells with compromised membrane integrity (Molecular Probes® Handbook, Section 14.2).

2.7. Microelectrode arrays

When an electrode is used to study the function of several surrounding neurons, the knowledge of the exact location of the measured neuron is lost (Smetters et al., 1999; Rochefort et al., 2009; Hogberg et al., 2011). However, by utilizing multiple electrodes to measure a large volume of a tissue or culture, the comparison of activity between different areas of the network as well as the activity transfer between these areas becomes possible (Smetters et al., 1999; Rochefort et al., 2009). The electrode arrays are well suited for the study of network activities, such as synchronous rhythms between neurons, because of the constructive interaction between the field potentials of synchronously active neurons (Rochefort et al., 2009).

In MEAs, the electrodes are spatially arranged within one plane. Electrodes of micrometer scale have the ability to record composite signals containing action potentials

superimposed over slower local field potentials (Rochefort et al., 2009; Gullo et al., 2010). The multiunit activity and the local field potential fluctuations can be separated from the MEA signal (Gullo et al., 2010). The multiunit activity measured by one electrode usually consists of the electrical activities of several cells (Wagenaar et al., 2006).

However, the spikes of the same cell have a distinctive wave shape which does not change unless the ion channels of that particular neuron are altered biochemically or spatially (Rochefort et al., 2009). The wave shapes of extracellular potential signals of somatic origin have been shown to have varying magnitudes and shapes from multiphasic to monophasic (Claverol-Tinture and Pine, 2002). Extracellular potential signals of neuritic origin, however, have been shown to be large, but monophasic negative (axons) or small monophasic positive (dendrites) (Claverol-Tinture and Pine, 2002). Due to the variety of factors affecting the wave forms of the recorded spikes, the time stamps of activity are used instead of individual wave forms when comparing different networks grown over electrode arrays (Morin et al., 2005).

Current density analysis can provide information on extracellular current flows (Claverol-Tinture and Pine, 2002), however, the signal forms recorded by the electrodes of MEA cannot be interpreted to gain information about the location of the signal source (Morin et al., 2005). Nonetheless, the ability of MEA technique to observe signal transmission and single cell activity levels, allows the high sensitivity to factors affecting network activity (Rochefort et al., 2009).

2.7.1. Bursting in the networks

Signal bursts are a commonly observed phenomenon during the extracellular electrode recordings of neural networks. Bursts recorded by the electrodes arise from the nearly simultaneous activity of several adjacent neurons (Wagenaar et al., 2006). Detecting and defining bursts as well as their properties have gained a great deal of attention (Canepari et al., 1997; Morin et al., 2005; Wagenaar et al., 2006; Sun et al., 2008). Bursts are often observed to occur synchronously between different recorded areas or propagating from one area to another (Canepari et al., 1997). Developmental stages characterized by differences in burstiness, temporal clustering of bursts, burst shapes and distributions of burst sizes have been shown to appear during the maturation of cultured networks (Wagenaar et al., 2006).

2.7.2. The effects of extracellular solution on activity observed with planar microelectrode arrays

The MEA platform is sensitive enough to allow the observation of changes in the activity due to differences in the ionic concentrations of extracellular solutions. The effects of different Ca^{2+}, K^{+} and Mg^{2+} ion concentrations on the signal recorded by MEAs has been studied (Canepari et al., 1997).

In these experiments, the low Ca^{2+} concentration was observed to cause asynchronous activity, while a higher Ca^{2+} concentration was observed to cause the synchronization of spikes seen as bursts of activity recorded by the electrodes (Canepari et al., 1997). An increasing Ca^{2+} concentration increased the temporal co-occurrence of spikes, ultimately leading to roughly periodic synchronized bursting (Canepari et al., 1997). The burst shape was also observed to be affected by the Ca^{2+} concentration and a change from a constant to biphasic and finally to oscillating burst form was associated with Ca^{2+} concentration elevation (Canepari et al., 1997).

K^{+} concentration was also shown to affect the network activity recorded by MEAs (Canepari et al., 1997). Both the frequency and burst shape of the synchronized bursts was shown to be affected by changes in K^{+} concentration (Canepari et al., 1997; Sun and Luhmann, 2007). By altering the K^{+} concentration the biphasic burst shape became distorted during the decreasing amplitude phase (Canepari et al., 1997). A more excitatory environment caused by higher K^{+} concentration has also been shown to distort the periodicity of bursting while simultaneously increasing the overall amount of activity (Canepari et al., 1997).

The effects of Mg^{2+} addition, on the other hand, were shown to depend on the Ca^{2+} concentration. If only the Mg^{2+} concentration was increased, the network became strongly silenced. However, if the Ca^{2+} concentration was increased simultaneously with Mg^{2+} concentration, only the periods between the occasional synchronous bursts became silent (Canepari et al., 1997).

In addition to the spontaneous network activity, the effects of pharmacological agents differ when applied in different extracellular solutions. This kind of effect was observed to depend on Ca^{2+} and Mg^{2+} concentrations (Canepari et al., 1997). A low Ca^{2+} concentration strongly decreased the blocking effect produced by competitive glutamate receptor antagonists (Canepari et al., 1997). A decrease in the effect of glutamate receptor

antagonist was also produced by the higher Mg^{2+} concentration, which is known to cause the blockage of glutamate receptors (Canepari et al., 1997).

Considering these observations it is important to control the ionic composition of the extracellular solution while performing and comparing activity recorded with the MEA platform.

2.8. Calcium imaging

2.8.1. The biological phenomena of neurons recorded by calcium imaging

The intracellular rise of calcium concentration in neurons is caused by the calcium entry via voltage-gated calcium channels or calcium-permeable ion channels coupled to ligand-gated receptors (Froemke et al., 2002). Because the intracellular calcium concentration in a resting neuron (30-150nM) is around 10,000 times smaller than the concentration of extracellular calcium (1-2mM), even short moment of membrane permeability to calcium ions is sufficient to generate a large intracellular calcium concentration rise (Knot et al., 2005). However, the calcium rise in cell cytoplasm can also be due to calcium release from intracellular calcium stores within the endoplasmic reticulum (Knot et al., 2005).

Several experiments have shown the correlation between calcium transients and the electrical activity of neurons by simultaneous calcium imaging and intracellular electrode recording (Smetters et al., 1999; Yoshida et al., 2001; Knot et al., 2005). It has been observed that during a neuronal action potential the amount of calcium entering the cell, and hence the extent of intracellular calcium concentration rise, is of the same size for each action potential occurring in that cell (Smetters et al., 1999). If the whole soma of the cell is measured, the calcium concentration rise produced by action potential, but not the calcium concentration rise associated with below action potential firing threshold depolarization, is enough to cause a 2-15% change in the measured fluorescence (Smetters et al., 1999).

While small increases of intracellular calcium concentration are usually associated with single spikes, bursting leads to a very strong intracellular calcium concentration increase (Opitz et al., 2002; Sun and Luhmann, 2007; Baltz et al., 2010). The intracellular calcium concentration rise occurring concurrently with a train of action potentials shows a cumulative nature of the calcium level signals as the calcium level rises caused by spikes in spike trains are superimposed on top of the preceding calcium level rise (Smetters et al.,

1999). However, in the case of train or burst like high rate activity, the influx of calcium reflected by fluorescence signal can be reduced due to the calcium indicator saturation (Smetters et al., 1999).

The kinetics of intracellular calcium concentration increases can exhibit various features. Commonly, the calcium transients can be classified as either transient or long-lasting ones (Knot et al., 2005). The transient rises are generally associated with single spikes and have been described with time-to-peak values of 5-50ms and decay times of 1-4s (Smetters et al., 1999). The intracellular calcium concentration changes can also exhibit an oscillatory nature (Kato-Negishi et al., 2003; Knot et al., 2005; Sun and Luhmann, 2007).

2.8.2. Principles of calcium ion sensitive optical probes and calcium imaging

Calcium imaging is an optical method requiring the use of a specific calcium ion sensitive fluorescent indicator. Calcium indicators are based on different calcium chelators, such as bis(2-aminophenoxy)ethane tetraacetic acid (BAPTA) or bis(2-aminoethyl ether)tetraacetic acid (EGTA), equipped with a conjugated fluorescent moiety (Knot et al., 2005). The calcium chelator based indicators bind to the free diffusible calcium (Molecular Probes® Handbook, Section 19.2). However, most of the intracellular calcium is not in a freely diffusible form but is bound by the intracellular buffers and compartmentalized to cellular organelles, such as the endoplasmic reticulum (Molecular Probes® Handbook, Section 19.2). As the calcium indicators themselves are calcium buffers, they can affect the intracellular calcium by binding too tightly or to too many calcium ions (Molecular Probes® Handbook, Section 19.2).

The molecular combination of the calcium chelator and the fluorescent structure allow the calcium indicator to produce a change in fluorescent properties upon binding to calcium. The type of change occurring in the fluorescent properties of the calcium indicator is different for different types of indicators (Grynkiewicz et al., 1985; Molecular Probes® Handbook, Section 19.2). A calcium indicator can be a single or a dual wavelength indicator. In a single wavelength indicator the calcium binding causes an increase in the intensity of the fluorescence of the molecule, while in dual wavelength indicator either the emission (i.e. Indo-1 indicator) or the absorbance (i.e. Fura-2 indicator) spectrum peak is shifted substantially (Grynkiewicz et al., 1985; Molecular Probes® Handbook, Section 19.2).

Dual wavelength indicators allow the use of ratiometric measurement methodology. In ratiometric measurements, the fluorescence of the calcium bound and the calcium free indicator forms are measured separately, by using two different emission or excitation wavelengths and their ratio is taken to minimize the effect of imaging artifacts (Molecular Probes® Handbook, Section 19.2). The imaging artifacts removed by using a ratiometric methodology are those arising from the variance of the indicator concentration in the cells (Molecular Probes® Handbook, Section 19.2). These variances can occur due to an uneven indicator loading, indicator leakage, photobleaching, and changes in the cell volume (Molecular Probes® Handbook, Section 19.2).

Calcium indicators generally have one of three different chemical forms. These forms affect their loading into cells. Calcium indicator salts and dextran conjugates are hydrophilic and thus membrane impermeant molecules (Molecular Probes® Handbook, Section 19.2). Due to the hydrophilic nature, both require invasive loading methods, but can be imaged within minutes after loading. The dextran conjugated calcium indicators are engineered to resist compartmentalization and cells loaded with dextran conjugated calcium indicators can be studied even over whole day (Molecular Probes® Handbook, Section 19.2). The AM ester forms of calcium indicators are hydrophobic and can be loaded to cells noninvasively (Knot et al., 2005; Molecular Probes® Handbook, Section 19.2). The AM masks the negative charges of the indicator, thus allowing it to cross lipid membranes (Molecular Probes® Handbook, Section 19.2). Once inside the cell, the ester bond between the indicator and the AM group is cleaved by intracellular esterases (Molecular Probes® Handbook, Section 19.2). After cleavage, the indicator is once again charged and unable to cross the cell membrane. This method allows the bulk loading of a cell population and thus enables the recording of multiple cells simultaneously.

Once loaded to the cell, the calcium indicator attains equilibrium between calcium free and calcium bound forms according to its equilibrium equation (see Equation 1 for calcium indicator equilibrium equation). The changes in the intracellular calcium concentration shift the equilibrium according to the equilibrium equation producing a change in fluorescence due to the change of the concentration of calcium free or calcium bound form of the indicator.

Equation 1

$$K = \frac{\left[Ca^{2+} \bullet indicator\right]}{\left[Ca^{2+}\right]\left[indicator\right]}$$

The dissociation constant of a calcium indicator describes how tightly the indicator binds to calcium (Molecular Probes® Handbook, Section 19.2). The changes in the indicator fluorescence are largest when the calcium ion concentration lies within 0.1-10 times the dissociation constant (Molecular Probes® Handbook, Section 19.2). Calcium indicators with varying properties of calcium binding have been engineered and they allow the study of intracellular calcium concentration over a large range (<50 nM to >50 μM) (Molecular Probes® Handbook, Section 19.2).

The actual dissociation constant of an indicator, however, depends on the environmental factors, such as pH and ionic strengths (Molecular Probes® Handbook, Section 19.2). Due to this feature, the dissociation constant needs to be measured for each cell type or cellular compartment studied to accurately calibrate the calcium levels for quantitative measurements (Molecular Probes® Handbook, Section 19.2).

Dissociation constant should be considered when choosing calcium indicator for the experiment (Molecular Probes® Handbook, Section 19.2). The calcium indicators of high affinity and low affinity have been engineered. The high affinity indicators have larger dissociation constant and they are suitable for the study of cytosolic calcium levels (Molecular Probes® Handbook, Section 19.2). However, as they bind to calcium more strongly they can more easily interfere with the intracellular calcium signaling (Molecular Probes® Handbook, Section 19.2). Low affinity calcium indicators, on the other hand, do not interfere as easily with intracellular calcium signaling, but produce weaker signals and are thus more suitable for studying cell compartments with high calcium concentrations (Molecular Probes® Handbook, Section 19.2).

Due to the transient nature of the calcium level changes, another important kinetic chemical property of the calcium indicator is the speed of binding described by the binding rate constant. If the calcium indicator binds too slowly to free calcium, it is not fast enough to reach its equilibrium before the calcium concentration begins to decrease (Molecular Probes® Handbook, Section 19.2). On the other hand, such molecules can stay fluorescent even if the intracellular calcium level has already decreased significantly. The signal produced by an indicator with too slow kinetics will not reflect the true intracellular calcium level changes and rapid calcium transients will not be seen.

3. Aims of the research

The first aim of this study was to optimize and characterize long-term fluorescent dye labeling protocols for living hESC-derived neural cells. The second aim of this study was to characterize the role of gap junctions in the neural network activity of maturing hESC-derived networks.

4. Materials and Methods

4.1. Cells

4.1.1. hESC -lines

A number of hESC-lines (Regea 08/056, 06/040, 06/015, 07/046, 08/013, 08/017, 08/023, HS181, HS362) were used in this study. The Regea-lines were derived at Regea while HS-lines were derived at the Karolinska University Hospital Huddinge, Karolinska Institutet, Sweden. Regea holds an approval from the Ethics Committee of Pirkanmaa Hospital District for derivation, characterization and differentiation of hESC-lines (RO5051, RO5116) as well as an approval (1426/32/300/05) of Valvira, the Finnish National Supervisory Authority for Welfare and Health, for research of embryos. Similarly, the Ethics Committee of the Karolinska Institute had approved the derivation, characterization, and differentiation of hESC-lines.

4.1.2. Derivation and maintenance of hESC -lines

The derivation and characterization of Regea-lines has been described (Rajala et al., 2010; Skottman, 2010). The maintenance culture of hESC lines was done as described earlier (Rajala et al., 2007). According to the registry entries at European Human Embryonic Stem Cell Registry (http://www.hescreg.eu/; 09.01.2012) the pluripotency of the hESC lines Regea 08/056, 08/017, 07/046, 06/040, 06/015, and 08/023 has been shown both *in vitro* and for Regea 06/040 and Regea 06/015 also *in vivo*. The derivation and culture conditions for HS-lines have been previously described (Hovatta et al., 2003). The pluripotency of the HS-lines has been shown *in vitro* and *in vivo* (Hovatta et al., 2003, Inzunza et al., 2004, Inzunza et al., 2005).

The undifferentiated hESC-lines were grown as colonies over mitotically inactivated human foreskin fibroblast (CRL-2429, ATTC, Manassas, VA) feeder cell layer. The hESC-culture medium is described in Table 1. The colonies were passaged and plated on top of fresh fibroblast layer at 5 to 7 day intervals. The maintenance of the undifferentiated hESC-lines, as described here, was performed by lab technicians. The hESC-lines were quality controlled with frequent gene and protein expression analysis, karyotype and mycoplasma assays.

4.1.3. Differentiation of hESCs towards neural lineage

The neural differentiation of hESC was performed as described by Lappalainen and colleagues (2010). Briefly, neural differentiation was initiated by mechanically cutting pieces from adherent undifferentiated hESC colonies. Subsequently, the cut pieces were transferred on to low attachment 6-well plates for suspension culture (Nunc, Thermo Fisher Scientific, Rochester, NY). During suspension culture, the differentiating colony pieces were fed with a defined neural differentiation medium (see Table 1 for components). After transfer to suspension culture, the cut colony pieces formed spherical floating neural aggregates, neurospheres. Neurospheres were cultured in the neural differentiation medium for 9-33 weeks during which the medium was 50% replaced 3 times a week. During this differentiation, neurospheres were mechanically passaged once a week.

4.1.4. Maturation of derived neural cells

For the final neural maturation step, the neurospheres were mechanically or enzymatically (described in detail later in 4.1.6) dissected and plated on to laminin (mouse or human, Sigma-Aldrich, St. Louis, MO) coated culture dishes or cover slips for adherent culture, while the basic fibroblast growth factor (bFGF) was withdrawn from the medium by changing the culture medium from neural differentiation medium to neural growth medium (see Table 1 for components). The medium was 50% replaced 2-3 times a week. The length of maturation step varied from 2 to 56 days.

Table 1 A list of cell culturing mediums and their compositions.

Medium	Components	Provider
hESC-culture medium	Dulbecco's modified Eagle's medium (DMEM)	Gibco Invitrogen, Carlsbad, CA
	20% knockout-Serum replacement	Gibco
	2mM GlutaMax	Gibco
	0.1mM minimal essential medium non-essential amino acids	Cambrex Bio Science, East Rutherford, NJ
	0.1mM betamercaptoethanol	Gibco
	50U/ml penicillin/streptomycin	Lonza Group Ltd, Switzerland
	8ng/ml human bFGF	Gibco
Neural differentiation medium	Neural growth medium 20ng/ml human bFGF	 Gibco
Neural growth medium	1:1 DMEM/F-12:Neurobasal media	Gibco
	2mM Glutamax	Gibco
	1xB27 supplement	Gibco
	1xN2 supplement	Gibco
	25U/ml penicillin and streptomycin	Lonza
Enhanced neural growth medium	Neural growth medium 4ng/ml human bFGF	 Gibco
	5ng/ml BNDF	Gibco

4.1.5. Preparing culture dishes and cover slips

Plastic culture dishes or glass cover slips were prepared for adherent cell culture by coating. Coating was performed by incubating laminin (10µg/ml for plastic, 20µg/ml for glass) for at least overnight in +4°C or two hours in +37°C, 5% CO_2, humidified atmosphere. Either the whole culture dish well was filled with laminin solution (~250µl/cm^2) or only part of the well bottom or cover slip by using droplet coating (50-100µl of laminin, Figure 1). After coating, the excess laminin was removed by suction and reused up to three times or until expiration (one month after preparing the aliquot).

Figure 1 Droplet coating. 50µl of laminin as a droplet in the center of a cell culture plate wells.

4.1.6. Dissecting and plating cells

Neurospheres were dissected either mechanically or enzymatically. In mechanical dissection, the neurospheres were cut with a sterile scalpel into barely observable pieces. The prepared culture dishes were filled with medium (1ml of medium per 1cm well radius) and several pieces were transferred to each well or cover slip. The amount of pieces per well or cover slip was kept constant in an experiment but varied from 8 to 16 between experiments. Plated culture dishes were placed into an incubator (+37°C, 5% CO_2, humidified atmosphere). During the following cell culturing period, 50% of the culturing medium was replaced with fresh medium 3-4 times a week.

In enzymatic dissection, the neurospheres were first transferred to an eppendorf tube and washed with 1ml of preheated, +37°C Dulbecco's modified phosphate buffered saline (DPBS, Lonza). After the neurospheres had sedimented to the bottom of the eppendorf tube, DPBS was removed and replaced with 200-500µl (based on the estimate of neurosphere size and amount) of preheated room temperature Trypple Select TM (Gibco). After 10-15 minutes incubation in +37 °C, the cells were suspensed by pipeting back and forth. Neural growth medium was added up to a volume of 1ml and suspensed cells were centrifuged (5min, 1400rpm, Eppendorf miniSpin). The resulting cell pellet was suspensed to neural growth medium. 8µl of the final cell suspension was transferred to a Nëubauer or Bürker chamber and cell counting was performed by averaging 3-4 major squares. The required cell suspension volume to achieve the desired cell count was calculated with Equation 2.

Equation 2

$$\frac{Final\_cell\_number}{Average\_of\_major\_squares * 10{,}000}$$

The required cell suspension volumes were transferred to each culture dish well or cover slip. The culture dish was placed into an incubator until the cells had attached (5-15min, confirmed with a phase contrast microscope). After cell attachment, the wells were filled with medium and placed into an incubator. During the following cell culturing period 50% medium was replaced with fresh medium 2-3 times a week.

In a set of experiments, the adherent cell cultures of the mature stage were dissected instead of neurospheres. This was performed by cutting the cultures mechanically or enzymatically as described previously for neurospheres. However, following modifications were added to enzymatic dissection: cells were washed as adherent, 200-400µl (depending on the cell density) of Trypple Select TM was added on each well and cell suspension was transferred to an eppendorf only after Trypple Select TM incubation.

4.2. Fluorescent microscopy

The cells labeled with fluorescent dyes or secondary antibodies (in immunocytochemistry) were visualized and imaged with a fluorescent microscope set (Olympus IX51 inverted microscope, PlanFLN 4x, 10x, 20x and 40x objectives, Olympus DP30BW CCD camera, 100W Halogen lamp light source). The light was filtered with U-MNU2 (excitation filter 360-370; emission filter 420; dicromatic filter 400), U-MNB2 (excitation filter 470-490; emission filter 520; dicromatic filter 500), U-MWG2 (excitation filter 550-510; emission filter 590; dicromatic filter 570), or U-N41023 (excitation filter 625-675; emission filter 710; dicromatic filter 680) filter cube.

The images were processed with Adobe Photoshop. Briefly, the grayscale images were converted to an RBG format and the output levels were adjusted to zero, except for the channel corresponding to the color of the fluorescent light. For example, to obtain color images from grayscale images taken by using the U-MNB2 filter set the red and blue channels output levels were adjusted to 0. The images taken from the same field of view with different filter sets were overlayed after converting them to corresponding color images to obtain composite images.

4.3. Fluorescent dyes

4.3.1. CellTracker Green

CellTracker Green CMFDA (5-chloromethylfluorescein diacetate, CT) is a fluorescent probe developed by Molecular Probes®. CT contains a fluorescent fluorescein structure attached to two acetate groups and a chrolomethyl group. Due to the additional groups CT is retained in living cells for several generations and is not transferred to other cells in the same population (Molecular Probes® Handbook, Section 14.2). As a fluorescent molecule the CT has an absorption maximum at 492nm and an emission maximum at 517nm (Molecular Probes® Handbook, Section 14.2). The fluorescent properties of CT are represented in Figure 2.

A 10mM CT stock was prepared from the solid CT (C2925, Lot 465545, 1mg, Molecular Probes Invitrogen, Finnzymes, Finland) by dissolving it to 215.1µl of DMSO (stored at -20^{o}C). On the day of use, the labeling medium was prepared by diluting the stock to fresh culture medium. The culture medium of cells was replaced with the labeling medium and incubated at +37^{o}C, 5% CO_2, humidified atmosphere. After incubation the labeling medium was replaced with fresh culture medium and the cells were imaged at varying periods after labeling.

4.3.2. DiD

1,1'-dioctadecyl-3,3,3',3'-tetramethylindodicarbocyanine perchlorate (DiD) is a lipophilic carbocyanine molecule. In water environment DiD is weakly fluorescent (Molecular Probes® Handbook, Section 14.4). As a lipophilic molecule DiD incorporates easily into membranes. In the lipid environment of the cell membrane DiD becomes strongly fluorescent (Molecular Probes® Handbook, Section 14.4). DiD has an absorption maximum at 644nm and an emission maximum at 665nm (Molecular Probes® Handbook, Section 14.4). The fluorescent properties of DiD are represented in Figure 2.

A 20mM DiD stock was prepared from the DiD oil (D-307, Lot 461358, 25mg, Molecular Probes Invitrogen). Labeling with DiD in coculturing experiments was performed in a same fashion as with CT (4.3.1). For this purpose a 5µM concentration was used in the labeling medium together with 2 hour incubation time. These parameters were optimized by Tiina Joki in her master's thesis work.

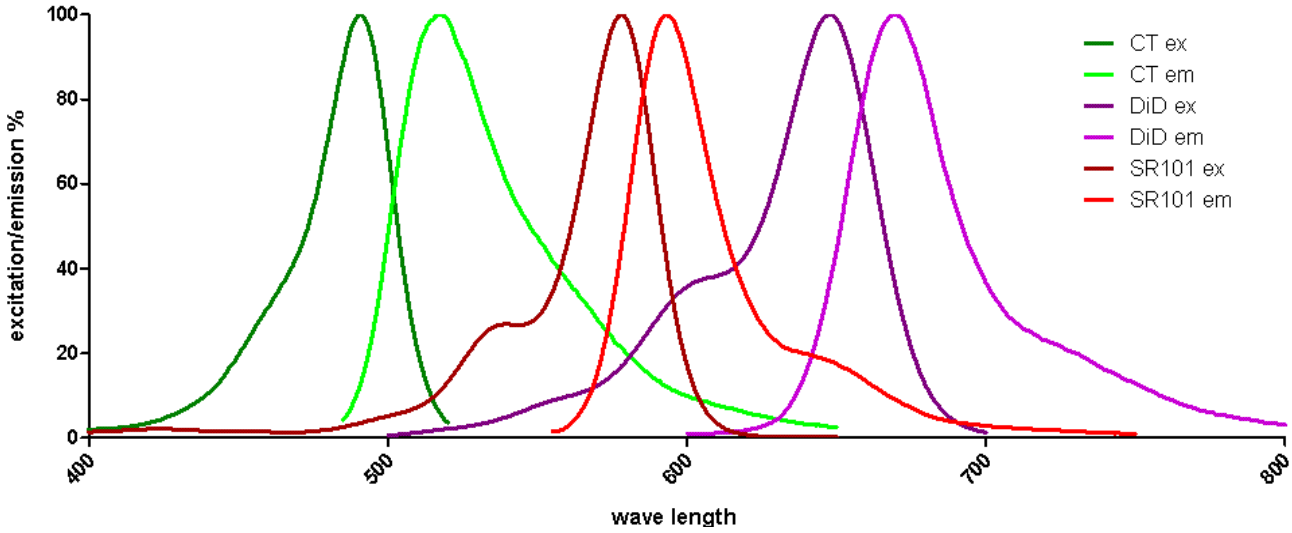

Figure 2 Fluorescent properties of CT, DiD and SR101. ex and em in the image refer to excitation and emission. Data for this graph was obtained from the manufacturer website (http://www.invitrogen.com; 03.12.2011).

4.3.3. Sulforhodamine

Sulforhodamine 101 (SR101) is a polar, water soluble, fluorescent molecule with an excitation maximum at 586 nm and an emission maximum at 605nm (Molecular Probes® Handbook, Section 14.3). The spectral properties of SR101 are represented in Figure 2. Previously, it has been reported that in brain slices a 100nm concentration of SR101 (Nimmerjahn et al., 2004; Kafitz et al., 2008) produces a homogenous cytoplasmic astrocytic staining which is stable for several hours (Nimmerjahn et al., 2004).

A 10mM SR101 stock was prepared from SR101 (S359, Lot 458872, 25mg, Molecular Probes Invitrogen) by dissolving to 4.12ml sterile H_2O (stored at +4 ^{o}C). Labeling with SR101 was performed in a same fashion as previously described for CT (4.3.1).

4.3.4. LIVE/DEAD

The LIVE/DEAD® Viability/Cytotoxicity Kit (L-3224, Molecular Probes Invitrogen) or the components of the kit purchased individually (Calcein AM; C1430, EthD-1; E1169, Molecular Probes Invitrogen) were used to study the effect on the cell viability. The LIVE/DEAD method is based on two dyes which become fluorescent after interacting with cells or their components. Calcein AM is inherently non-fluorescent and upon entering the cell it is converted to a fluorescent molecule by the intracellular esterases (Molecular Probes® Handbook, Section 15.2). Ethidium homodimer (EthD-1) does not diffuse through plasma membrane as Calcein AM but it will enter cells with a damaged plasma membrane (Molecular Probes® Handbook, Section 15.2). Upon binding to nucleic acid, a 40-fold enhancement of fluorescence of EthD-1 will take place (Molecular Probes® Handbook,

Section 15.2). The fluorescence from by Calcein AM is hence relative to the cellular esterase activity while that of EthD-1 is relative to accessible DNA, indicating live and dead cells, respectively.

To perform the LIVE/DEAD staining for microscopy analysis, the stock solutions of Calcein AM and EthD-1 were removed from -20^{o}C and diluted to preheated +37^{o}C neural growth medium to achieve final concentrations of 0.1μM and 0.5μM, respectively. The medium was removed and replaced with a freshly made labeling solution. After 30 minutes of dark incubation the cells were imaged with a fluorescence microscope.

In order to quantify the fluorescence images, a total of 5 images from 2 adjacent well were analyzed. Analysis was performed by manually counting the number of Calcein AM and EthD-1 labeled cells. The percentage of dead cells was obtained by dividing the mean of EthD-1 labeled cells with the mean of Calcein AM labeled cells.

4.4. Immunocytochemistry

CT, SR101 or DiD stained adherent cultures were studied immunocytochemically to determine the specificity of staining. Medium was removed and cells were rinsed with room temperature Dulbecco's phospahe buffered saline (DPBS, Bio Whittaker, MD, USA) to prepare the cells for fixing. For fixation, DPBS was replaced with +4^{o}C 4% paraformaldehyde and incubated for 15 minutes in room temperature. Paraformaldehyde was washed twice with DPBS and the cytochemical stainings were done immediately or the culture plate was stored in +4^{o}C for later immunocytochemistry. To prevent the unspecific binding of antibodies, cells were permeabilized with 0.1% Triton X-100 (Sigma) and blocked with 10% normal donkey serum (NDS, Millipore) in 1% bovine serum albumin (BSA, Sigma) in DPBS. Primary antibodies were diluted to 1% NDS, 1% BSA in DPBS with 0.1% Triton X-100 as permeabilizing agent unless stated otherwise. The primary antibody solution was kept on cells over night at +4^{o}C, unless stated otherwise. As the secondary antibodies are conjugated to photosensitive groups, the cultures and reagents were kept in dark during following phases. After primary antibody incubation, the excess primary antibodies were removed by washing with 1% BSA in DPBS and the secondary antibodies were added in 1% BSA in DPBS and incubated on shaker at room temperature for one hour. The excess secondary antibodies were removed by washing three times with PBS and traces of salts were removed by washing twice with phosphate buffer without saline. For nuclear staining and mounting, 7μl Vectashield with 4',6-diamidino-2-

phenylindole (DAPI, H1200, Vector laboratories, Peterborough, UK) was added and the sample was covered with a glass cover slip.

4.4.1. Antibodies

The primary antibodies used were anti-MAP-2 (rabbit, 1:600, AB5622, Millipore, Finland) for detecting neuronal cells as well as their processes, anti-GFAP (sheep, 1:600, AF2594, RandD Systems, Minnepolis, MN) for detecting astrocytes and anti-Ki-67 (rabbit, 1:800, AB9260, Millipore) for detecting proliferating cells. Secondary antibodies used were AlexaFluor-488, -568 or -680 conjugates of anti-mouse, anti-rabbit or anti-sheep secondary antibodies (1:600, Molecular Probes Invitrogen).

4.4.2. Proliferation assay

In order to quantify the results for one experiment, a minimum of 2 parallel wells were imaged (minimum of 3 images per well). The DAPI and Ki-67 positive cell nuclei were counted for each image and the amount of Ki-67 positive nuclei was divided by the amount of DAPI labeled nuclei. This was performed for each image and the obtained values are presented in the results.

4.4.3. Different permeabilizations

Permeabilizations in immunocytochemistry were performed to guarantee the access of antibodies to their intracellular targets. In order to avoid fluorescent dye loss while keeping the cytochemical staining optimal, two different permeabilizers were studied. Triton X-100 was used as 0.1% dilution in blocking and primary antibody solutions. Saponin (7900-25g, Sigma-Aldrich) was used as a 1% and 0.1% solution and it was added to blocking, primary antibody, washing and to secondary antibody solutions. Immunocytochemical staining protocol was also performed with no permeabilization.

4.5. Microelectrode Array System

4.5.1. Equipment

The extracellular local field potentials produced by electrical activity of neurons were studied by culturing cells on MEA-dishes. MEA-dishes contained an integrated array of insulated titanium nitride microelectrodes. The microelectrode ends were permanently coated with a conducting material, platinum black. Three types of MEA-dishes with different electrode configurations and cell culture areas were utilized (see Table 2, all purchased from Multi Channel Systems, MCS, Reutlingen, Germany). The microelectrodes had 30µm diameter and 200µm inter-electrode distance on all MEA-

dishes. The coated ends of the electrodes form an array in the center of the cell culturing area and their opposite ends are at the periphery of the MEA-dish. During recordings the peripheral ends of the electrodes were connected to an external preamplifier. The preamplifier relayed the measured voltage signal to a filter and further to an analog to digital converter. The measured signal was processed and stored digitally.

Table 2 List of microelectrode array dish types used.

MEA-dish type	Number of cell culture areas	Cell culture area	Electrodes per culture area
standard	1	Permanent glass ring	59 + 1 reference
without glass ring	1	Removable PDMS	59 + 1 reference
6-well	6	Removable PDMS	9 + 1 reference

The microelectrode measurements were performed using MEA-dishes sealed in a laminar flow hood with 70% ethanol cleaned semi-permeable membrane (ALA MEA-MEM, ALA Scientific Instruments Inc., Westbury, NY) for standard MEA-dishes and for MEA-dishes without glass ring. 6-well MEA-dishes were sealed with a 70% ethanol cleaned glass circle. Dishes were sealed to avoid contamination. After sealing, MEA-dishes were placed into a faraday cage protected amplifier (MEA-1060BC, MCS) which made contacts with the peripheral ends of the electrodes on the MEA-dish. The MEA-dish was kept warm with an external heater unit (TC02, MCS) set to +38^{o}C. After measurements, the seals were removed, cleaned with 70% ethanol and reused, while the MEA-dishes containing cell cultures were returned to incubator.

After placing the MEA-dish into the amplifier, the system was allowed to settle for one minute after which the recording was started. The measured signals were preamplified with MEA1060-Inv-BC (gain 53, MCS) and prefiltered with FA60SBC (gain 20, MCS) producing signal with 1100 gain and 1Hz - 8 kHz bandwith. Analog to digital conversion was performed by MC_card (MCS) with 20kHz sampling frequency. The data acquisition card was controlled via MC_Rack software (MCS). The digitalized recordings were further processed by removing mains noise (50Hz band reject) and base line fluctuations (200Hz high pass) with 2nd order Butterworth filter. Spike detection was performed online with MC_Rack software by using threshold based detection (5 times standard deviation of noise level). Both, the electrode raw data and detected spikes were saved for analysis. Signals were recorded for 5 minutes 1-3 times a week for each MEA.

4.5.2. Coating, plating and cell culturing

For MEA experiments, the dishes were cleaned with 70% ethanol and dried in a laminar flow hood. Dry MEA-dishes were first coated with polyethyleneimine (PEI, 0.1%, Sigma-

Aldrich) as 1ml, 100µl or 50µl droplet for at least overnight in +4°C or 2 hours in +37°C and washed with sterile water. If the MEA-dish did not contain PDMS, it was sterilized with UV light inside laminar flow for at least 30 minutes at room temperature before or during the first coating. The second coating was performed with laminin (20ug/ml, mouse or human, Sigma) as 1ml, 100µl or 50µl droplet for at least overnight in +4°C or 2 hours in +37°C. If MEA-dish contained a PDMS, the droplet coating method was always used. Laminin was not reused and the aliquot was used within one month of preparation.

The cells were prepared mechanically or enzymatically as described previously (4.1.6) and transferred to the electrode area of MEA-dishes. The co-cultures of cells labeled with different fluorescent dyes were produced by plating single cell suspension from both labeled cultures to same cell growth area. After 3-5 days of culturing in neural growth medium, the medium was replaced with enhanced neural growth medium (Table 1) which was 50% replaced with fresh enhanced neural growth medium 3-4 times a week.

If the cells detached, neurites were destroyed, or no signal was observed during the first two weeks, the neural networks were determined as deficient and cultures were discarded. After use, the MEA-dishes were washed with distilled water and placed into Tergazyme solution (4g/200ml, Z273287, Sigma-Aldrich) for at least overnight. Tergazyme was washed off with distilled water and the MEA-dishes were air dried and stored for reuse.

When testing the effect of HEPES buffer (17-737E, 1M, Lonza) on neural network development, cell cultures were divided into three groups. Two of the groups were plated as described above, while the third (Hepes 1) was plated in neural growth medium containing 5mM HEPES pH adjusted to 7.4 with NaOH. After 9 days of maturation on MEA, one of the groups of cell cultures (Hepes 2) plated without HEPES was transferred to HEPES containing medium, while the other (control) was kept in neural growth medium lacking HEPES and the microelectrode array measurements were begun. The mediums were 50% replaced 3-4 times a week.

When testing the effect of Ringer solution (44µM KH_2PO_4, 20mM HEPES, 4.2mM $NaHCO_3$, 5mM glucose, 1mM $CaCl_2$, 1.2mM $MgCl_2$, 137mM NaCl, 5mM KCl, pH adjusted to 7.4 with NaOH) on signaling of the neural network, the cell culturing was performed as described above. The baseline was first measured in the culturing medium, after which the medium was replaced with Ringer solution or fresh neural growth medium. The networks were allowed to settle in the changed medium for an hour after. This was followed by a second measurement and medium change back to enhanced neural growth medium. The

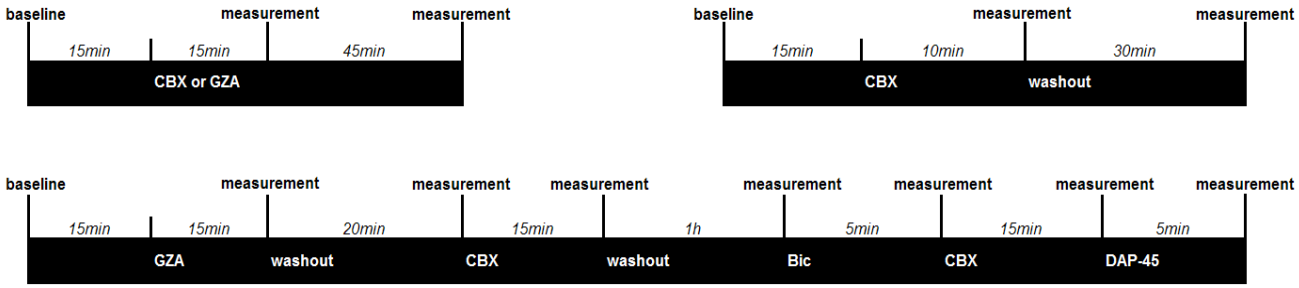

Figure 3 Timelines for drug applications and microelectrode array measurements. The up left corner timeline is for pharmacological experiment 1, the up right corner for pharmacological experiment 2 and the bottom time line is for pharmacological experiment 3. Abbreviations: carbenoxolone (CBX), glycyrrhizic acid (GZA), bicuculline (Bic).

experiment was repeated with the same cultures after 3 days and the incubation time after the medium change was extended to two hours.

4.5.3. Performing pharmacological testing

Three series of pharmacological experiments were performed on hESC-derived neural networks cultured over MEAs. A five minute baseline measurement was performed before applying any drugs. The drugs were applied by adding a very small volume (≤ 5µl) of the drug stock solution to the cell culturing solution of MEA-dish (800µl). After drug application, MEA-dishes were incubated in an incubator (+37^{o}C, 5% CO_2, humidified atmosphere, times in Figure 3) and the response was measured by obtaining signal from the microelectrodes for 5 minutes. The washouts were performed by replacing the medium with fresh preheated (+37^{o}C) cell culturing medium. The timelines and drug application sequences with respect to measurements can be seen from the Figure 3. The final drug concentration were 25µM carbenoxolone (CBX, C4790, Sigma-Aldrich), 25µM glycyrrhizic acid (GZA, 50531, Sigma-Aldrich), bicuculline (Bic, 14343, Sigma), DAP-45 (Asc-003, Ascent Scientific, UK).

4.5.4. Data Analysis

The data resulting from the online spike detection during MEA measurements was further analyzed offline. The spike counts and time stamps on each electrode were extracted with NeuroExplorer (Nex Technologies, Littleton, MA) software and collected to Excel files and combined to raster plots. Electrodes containing less than five spikes in each recording were considered inactive and removed from further analysis. Analyzed parameters were: the number of active electrodes per electrode array, the number of spikes recorded by the whole electrode array (total spikes), and the mean number of spikes per electrode.

4.6. Ca2+ imaging

4.6.1. Coating, plating and cell culturing

13mm diameter glass cover slips were cleansed with 90% ethanol and dried. The dry cover slips were transferred to 24 or 4 well plates and coated with laminin (20µg/ml) which was incubated for overnight in +4^{o}C. Cells were plated as single cells or aggregates, as described earlier (4.1.6), onto prepared cover slips and cultured similarly as when grown on plastic well plates (4.1.4). After imaging the cover slips were discarded.

4.6.2. Labeling cells with calcium indicator

Intracellular calcium transients were visualized with calcium indicator Fura-2 acetoxymethyl (Fura-2 AM, Lot: 781648, F1221, Molecular Probes Invitrogen). Fura-2 is a charged molecule but the AM conjugated version the charges are masked by the AM groups. Once the dye has permeated the cell plasma membrane, intracellular esterases cleave the AM groups leaving the fluorescent dye trapped inside the cell.

Cover slips containing cells were transferred to a small petridish containing 1ml of Ringer solution (described earlier in 4.5.2). Fura-2 AM stock (1mM dissolved to DMSO) was added to 4µM concentration. Fura-2 AM was incubated in room temperature (+22^{o}C) for 30 minutes. Subsequently, cover slips were removed from the loading solution and attached to an open diamond bath recording chamber (RC-25) with vacuum glue. The chamber was filled with Ringer solution and attached to platform (P3). The platform was mounted with a stage adapter to micromanipulator (SM 5-9, Luigs and Neumann, Ratingen, Germany) controlled stage of the imaging microscope (20x Olympus UApo/340 objective, Olympus IX51 microscope) and fluorescence was confirmed via microscope oculars.

4.6.3. Measurement of calcium dynamics

Two image sets were captured with TillVisiON. The first image set was captured by using 340nm excitation wave length and the second by using 380nm wavelength. The emission of both series was gathered via the same filter (Fura-2 bsp400LP, emitter 510/80nm). Images for both sets (340nm and 380nm excitation) were captured at 1Hz. No binning was used.

The excitation wavelength was produced with software controlled monochromator (Polychrome V, TILL Photonics, Gräfelfing, Germany) and emission was filtered with a filter cube (Fura-2 bsp400LP, emitter 510/80nm). The emitted fluorescence signal was

imaged with a cooled charge-coupled device (CCD) camera (iXion+ 885, Andor Technology, Belfast, Ireland) which was controlled by software (TILLvisON v.4.5.65, TILL Photonics). After confirming the presence of fluorescence and cells, the perfusion chamber was connected to a gravity fed perfusion system with peristaltic suction pump (Minipuls 3, Gilson, Limburg, Germany).

4.6.4. Analysis of calcium dynamics

Curves for intracellular calcium levels were obtained from the captured image series with TillVisiON. First, a sequence of ratio (Equation 3) images was constructed from the two captured image sets (no background correction, intensities lower than 30 clipped to zero, scaling with a factor of 1000). The differential fluorescence (Equation 4) image series were obtained from the ratio series (scaling with a factor of 1000). Regions of interests (ROIs) were hand drawn in TillVisiON and fluorescence kinetics (mean gray value) for each ROI were exported to excel files. The fluorescence trace of the background ROI was averaged with a kernel of 10 and subtracted from each fluorescence trace. The resulting values were multiplied by the average value of the background fluorescence. The fluorescence change trace for each ROI was then visualized and analyzed manually.

Equation 3

$$Ratio = ScaleFactor * \frac{F_{340}}{F_{380}}$$

Equation 4

$$DeltaF = ScaleFactor * \frac{F(t) - F_0}{F_0}$$

4.7. Pharmacological substances

Pharmacological substances were applied via the gravitation fed perfusion system. Before perfusing the cells, the substances were diluted to their final concentrations. If two substances were applied simultaneously, only one perfusion channel was used to apply the perfusion solution containing both agents in defined concentrations. KCl (250µM, 30mM, 50mM or 70mM, P9541-500G, Sigma) was applied to cause the opening of the voltage gated calcium channels via membrane depolarization and hence to identify neurons. $GABA_A$ receptor blocker bicuculline (Bic, 10µM or 50µM) was applied to cause the bicuculline-induced intracellular calcium rises described by Arumugam (2008). Carbenoxolone (25µM, CBX) was used to block the gap junctions. Glycyrrhizic acid

(25µM, GZA) was used as a control compound for CBX as it has been described to cause similar unspecific effects as the gap junction blocker CBX (Rouach et al., 2003). On the day of use, all applied substances were diluted to the Ringer perfusion solution described earlier (4.5.2).

5. Results

5.1. LIVE-Colors

5.1.1. CellTracker

5.1.1.1 **Optimizing CT labeling**

In order to find out optimal labeling parameters, several CT dye concentrations were studied together with a group of different incubation times. The manual of the dye (CellTracker Probes for Long-Term Tracing of Living Cells, Invitrogen) recommended the use of 5-25μM dye concentrations and 15-45 minute incubation times to achieve labeling for more than 3 days. The dye concentration was recommended to be kept as low as

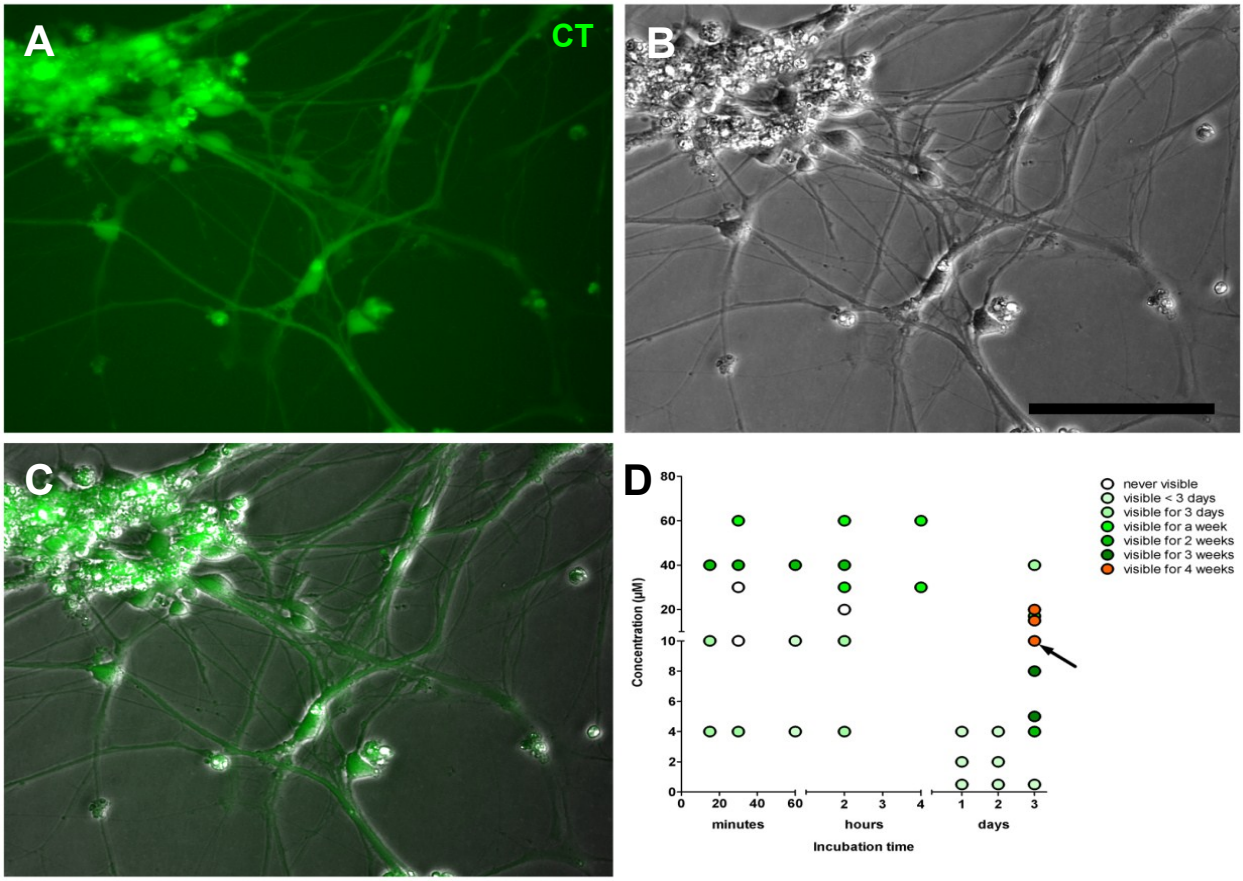

Figure 4 Labeling with CellTracker. Fluorescent live cells labeled by the optimal CT labeling parameters: 10μM concentration with 3 days incubation time (A). Phase contrast image of the same cells (B). Overlay of the images taken with fluorescence and phase contrast (C). Combinations of concentrations and incubation times studied during CT labeling optimization (D). The marks filled with white represent parameters for which no labeling was observed. Marks filled from light green to dark green and finally to orange represent the time period for which the fluorescent was observable after labeling. The arrow points to the mark representing the combination of optimum parameters for long term labeling. The scaling in A, B and C is the same and the scale bar in B is 100μm.

possible to avoid changes in cellular physiology. The dye concentrations used in this set of experiments ranged from 0.5μM to 60μM and the incubation times from 15 minutes to 72 hours. The exact combinations of parameters can be found from the Figure 4D.

During the first experiments, a concentration range from 4μM to 40μM was studied with incubation times from 15 minutes to 2 hours. The labeling was observed to be visible at the 3 week time point only with the highest (40μM) concentration and hence the CT concentration range was increased to 10-60μM while similar incubation times, from 30 minutes to 4 hours, were studied in the following experiments.

With low incubation times and high concentrations the staining was initially clearly observable but diminished greatly during the first week. By using the highest concentration it was possible to achieve labeling which was observable for 12 days.

Because the aim was to achieve labeling for several weeks, a new labeling strategy with low dye concentrations and very long incubation times was studied. The huge increase in the incubation time, days rather than hours, increased the dye retention time up to several weeks and hence further experiments were carried out by using 72 hours (3 days) incubation time. Subsequent experiments, with concentration ranges from 2μM to 20μM, revealed that the lowest concentration producing properly observable labeling of the cell morphology up to 4 weeks follow up times was 10μM labeling solution (Figure 4D). These optimal CT labeling parameters, 10μM, 72h, enabled the labeling of both, cell bodies and processes.

5.1.1.2 **The effect of CT staining on cell viability and proliferation**

As the labeling parameters lied outside the range recommended by the CT provider, the effect on cell viability was assessed. Viability was studied by performing a LIVE/DEAD staining for cells incubated for 72 hours with 10μM concentration of CT. The LIVE/DEAD staining was performed 4 and 15 days after labeling to reveal the acute labeling effect and long term dye retaining effect. An example of images captured for viability analysis can be seen in the Figure 5A, and the data from cell counting are depicted in Figure 5B. No statistically significant differences were found between control cells and CT labeled cells (Mann Whitney -test, $p > 0.05$) in either time point.

In addition to viability, the possible effect of CT on cell proliferation was studied. The cells were fixed either 6-7 or 11-13 days after the beginning of 72 hour 10μM dye incubation period and the proliferation was studied by immunostaining against Ki-67, a marker of

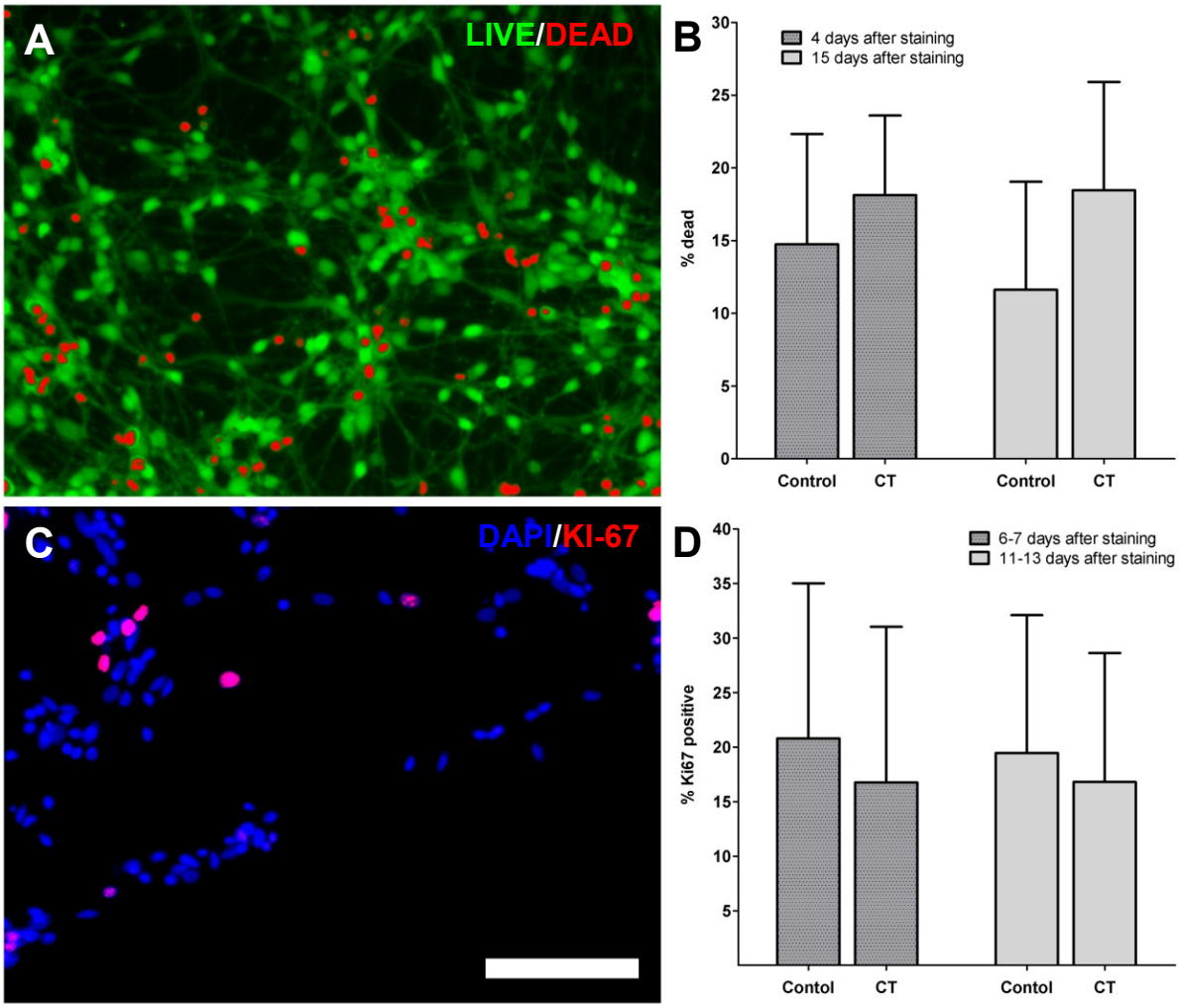

Figure 5 The effects of CT on cell cytochemistry. An example image from the series of images captured for viability analysis (A). Red: dead cell labeled by EthD-1. Green: alive cells labeled by Calcein AM. Data gathered from the cell counting performed during viability assay (B). Bars represent the mean values while whiskers represent the standard deviation. Similarly, an example image from the series of images captured for proliferation analysis (C). Blue: cell nuclei labeled with DAPI. Red: Proliferating cell nuclei labeled by Ki-67. The data gathered from the cell counting of proliferation experiments. Bars represent the mean values while whiskers represent the standard deviation. Scaling is same for A and C. The scalebar in C is 200µm.

dividing cell nucleus. An example image of the immunocytochemical staining against Ki-67 is presented in Figure 5C and the data from cell counting is presented in Figure 5D. No statistically significant differences were found between the control cells and CT labeled cells (Mann Whitney -test, $p > 0.05$) in either time point.

5.1.1.3 **Optimizing immunocytochemical staining protocol for LIVE-Colors**

Because some of the fluorescent dyes used in label living cells, such as DiD, attach to the cell membrane, they are very sensitive to permeabilizations which are harsh on the cell membrane. The original immunocytochemical staining protocol contained permeabilization with Triton-X 100 (Figure 6A) and the protocol was modified to use a milder permeabilitant,

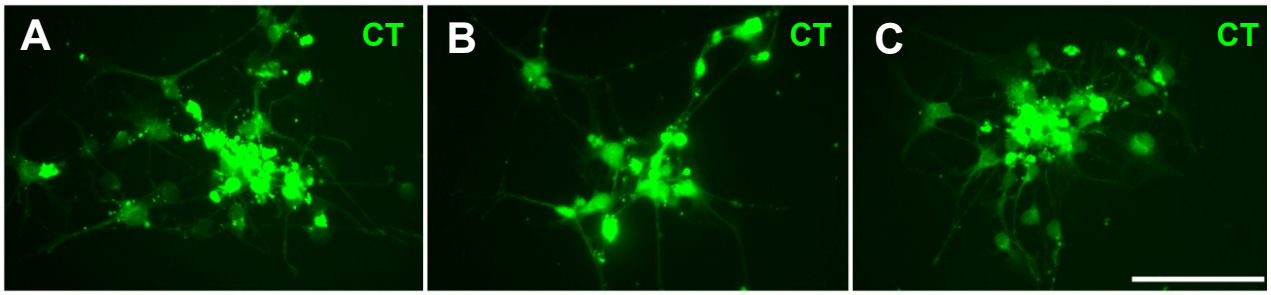

Figure 6 CellTracker retainment in different permeabilizations. 0.1% Triton-X permeabilization for over night (A). 1% saponin permeabilization for 3 hours (B). 0.1% saponin permeabilization for over night (C). Scale bar is 200µm and same for all images.

saponin. The immunocytochemistry protocol was first modified by using 0.1% saponin in all steps from blocking to secondary antibody incubation. This modified form of the immunocytochemical staining protocol allowed successful immunostaining and retainment of the CT label (Figure 6C). However, as this protocol did not allow good retainment of the other fluorescent dyes studied in this project, the protocol was further modified.

The primary antibody incubation time was the longest incubation during the immunocytochemical staining protocol and was hypothesized to be the reason behind the diffusion of other fluorescent labels away from the fixed cells. In order to study this perspective, the immunocytochemical staining protocol was modified by decreasing the primary antibody incubation time from overnight (ON) to 3 hours. Simultaneously, the saponin was increased to 1% to provide a more efficient permeabilization of the primary antibodies. This modification allowed the retainment of CT (Figure 6B) and was found not

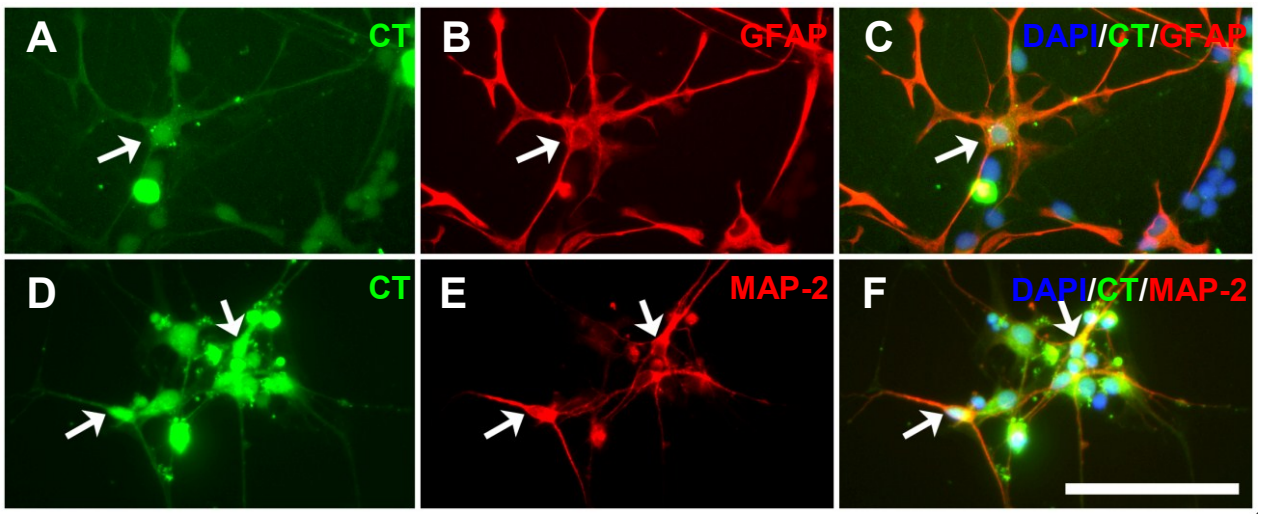

Figure 7 Immunocytochemistry of CT labeled cells. Immunocytochemistry was performed against GFAP (A,B,C) and MAP-2 (D,E,F) with 1% saponin permeabilization and 3 hour primary antibody incubation. The arrows point to CT labeled GFAP positive or MAP-2 positive cells. Scaling is same for all images and the scale bar is 100µm.

to disturb the immunocytochemical staining performed against GFAP (Figure 7B) or MAP-2 (Figure 7E). When the results from this experiment (3 experiments with 3-4 parallel cell culture wells in each) were compared to the results performed with 0.1% saponin permeabilization with overnight primary antibody incubation (4 experiments with 3 parallel cell culture wells in each), it was observed that the unspecific background staining for MAP-2 was more profound in the latter. No clear differences in the immunocytochemistry against GFAP were observed between these two immunocytochemistry protocols. Both 0.1% and 1% saponin permeabilizations were later studied in combination with antibody incubation times of 3, 6, 12 and 24 hours (1 experiment with 3 parallel cell culture wells). From this experiment it was observed that longer than 3 hour primary antibody incubation time did not clearly improve the immunocytochemical staining. Hence, 1% saponin permeabilization with 3 hour primary antibody incubation could be argued to be, out of the studied parameters, the most suitable for permeabilization modified immunocytochemistry (representative images in Figure 7).

5.1.1.4 **Characterizing the ability of CT to stain all cells**

When comparing the fluorescent images of CT labeled cell populations to their transmission light images, it seemed that CT would label all the cells in the population. CT stained cells were fixed and stained with DAPI to see whether CT is able to stain all the cells. Cells were counted and the percentage of CT labeled cells from DAPI stained cells was 94% (1 experiment, 604 cells, 6 imaged areas from 2 parallel wells). Hence, it can be

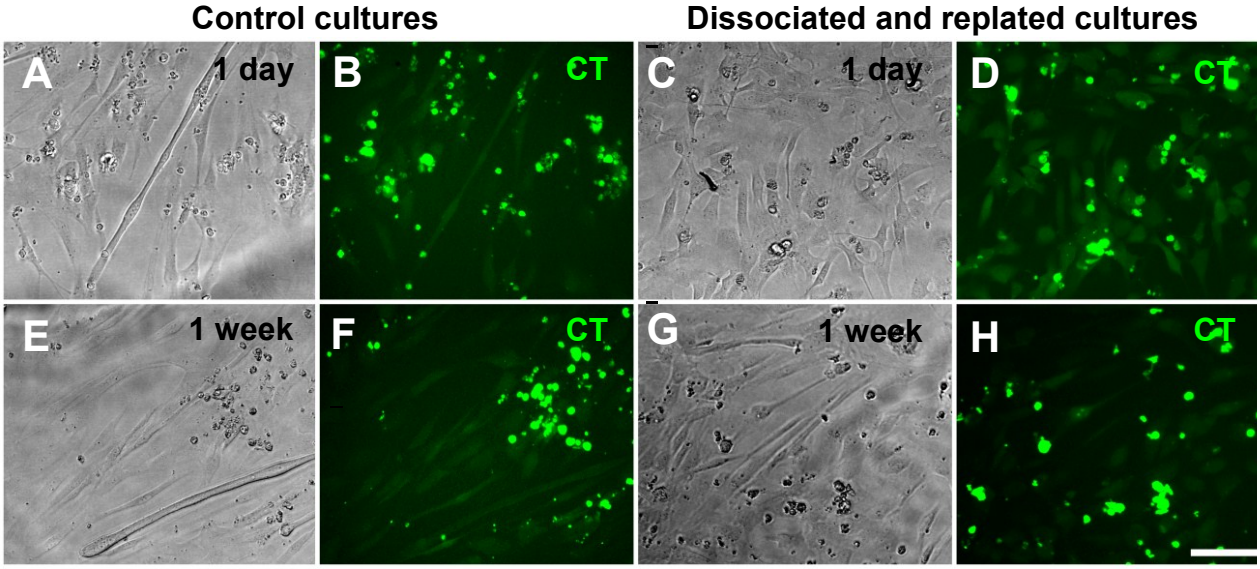

Figure 8 Replating CT labeled cells. CT labeled cells were dissociated and replated after being stained as adherent cultures. Control cultures were labeled but not dissociated. Control (A, B) and replated (C, D) cultures of CT labeled cells after one day and one week (E, F, G ,H) after dissociating the replated cells. Scaling is same for all images and the scale bar in image H is 100µm.

argued that CT labels virtually all cells of the differentiated populations.

5.1.1.5 **The suitability of CT for replating and co-culturing**

To further asses the suitability of CT for labeling mixed cell cultures, the behavior of the labeling in the process of dissociating and replating previously stained cells was studied. It was observed that CT is retained during dissociation and replating acutely (Figure 8D) as well as after longer time period (Figure 8H). Furthermore, it was observed that the background fluorescence is diminished as prelabeled cells were replated (Figure 8D). No clear difference in the intensity of the fluorescence was observed between control and replated cultures (1 experiment with 4 parallel cell culture wells). Thu,s CT is suitable for applications where the cells are needed to be dissociated and replated.

To study the suitability of CT for coculturing with other fluorescent label, DiD, mixed cultures were formed and followed with fluorescence microscopy. The cells from different adherent cultures labeled with different fluorescent dyes did not seem to avoid each other and grew as a mixed network (Figure 9). Initially, the dyes seemed to be retained in different cells (Figure 9B) but during the long term coculturing dyes became partially colocalized and granular (Figure 9E).

The effect of CT and DiD labeling on the formation of the network activity was studied by plating mixed cultures of prelabeled cells over MEA (Figure 10). After plating, the

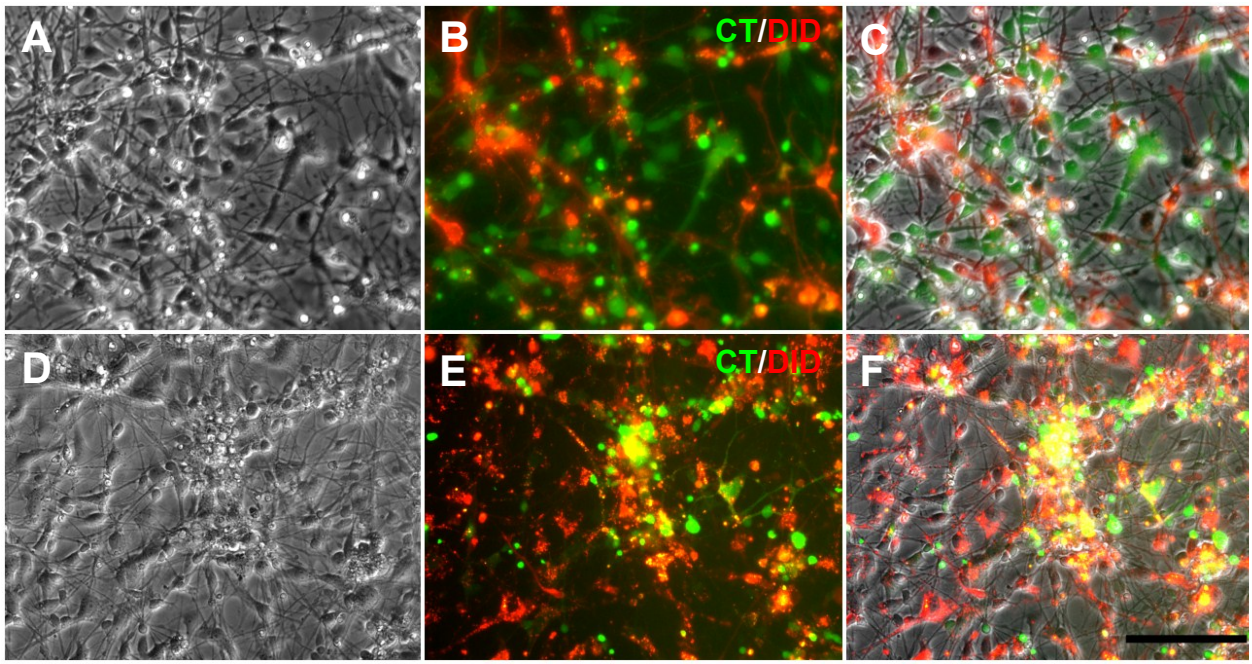

Figure 9 Mixed cocultures of cells labeled separately with CT or DiD. Phase contrast (A), combined fluorescence (B) and overlay of phase contrast and fluorescence images (C) from cocultures of two cell populations 4 days after mixing. A corresponding image serie 17 days after mixing (D, E, F). Scaling is same for all images and the scale bar in F is 100µm.

development of the activity was followed by sequential measurements. During this follow up period, the mixed cocultures developed first single spikes and later semisynchronous trains. From these observations, it can be deduced that the fluorescent labeling with CT and DiD does not prevent the development of electrogenic properties of hESC derived neurons. On the basis of semisynchronous activity between different electrodes, it can also be argued that the labeling with CT and DiD, as well as coculturing in a mixed form, does not prevent the formation of network connections between the hESC derived neurons. On the basis of semisynchronous activity between different electrodes, it can be also argued that the labeling with CT and DiD, as well as coculturing in a mixed form, does not prevent the formation of network connections between the hESC derived neurons.

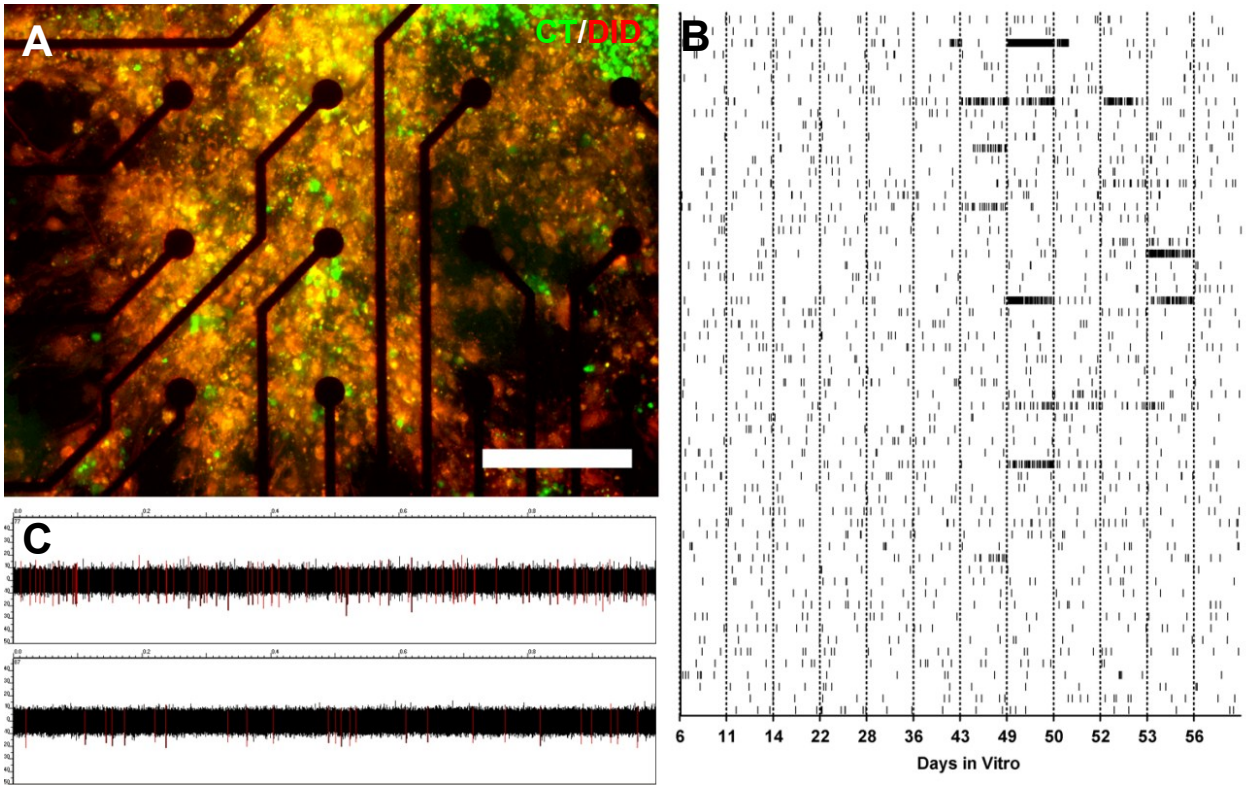

Figure 10 Functionality of the neural network formed by mixed cultures. A dense cell network formed by cells labeled with different fluorescent dyes growing over a microelectrode array (A). The scale bar in image A is 100µm. Development of network activity from single spikes to semisynchronous spike trains (B). Each vertical tic in B represents a spike while each row represents activity from single microelectrode. The activity between two vertical lines contains spikes recorded during 5 minute recording at each measurement day (x axis). A close up view of semisynchronous training from two adjacent electrodes in a mixed coculture of CT and DiD labeled cells (C). The red lines in C represent spikes.

5.1.2. Sulforhodamine 101

5.1.2.1 **Optimization**

Several hESC -lines (HS362, HS181, Regea 06/015, 06/040, 07/046, 08/013, 08/017, 08/023) were stained with Sulforhodamine 101 (SR101) at varying points of neural differentiation (9-33 weeks) as well as at varying points of neural maturation (2-56 days). The staining parameters used varied for incubation time from 5 minutes to 72 hours and for concentration from 0.5µM to 100µM. Not all staining parameters were studied with all hESC -lines or with the whole range of neural differentiation and maturation times. Figure 11 contains the parameters studied with two different hESC-lines.

The neural maturation time seemed to be a confounding factor and hence cell cultures were divided into groups based on the maturation time. Groups were termed immature and mature, having less than 5 days or more than 13 days long maturation step, respectively. The effect of maturation time can be seen in Figure 11 between the labeling for immature and mature cultures of Regea 08/023 -line.

In addition, a difference in successful staining parameters was found between different hESC -lines and is demonstrated in Figure 11. The staining seemed to be random with respect to the time differentiated before plating. However, based on successful staining on several cultures, the recommended labeling parameters for SR101 would be 10µM concentration with 8 hours incubation time.

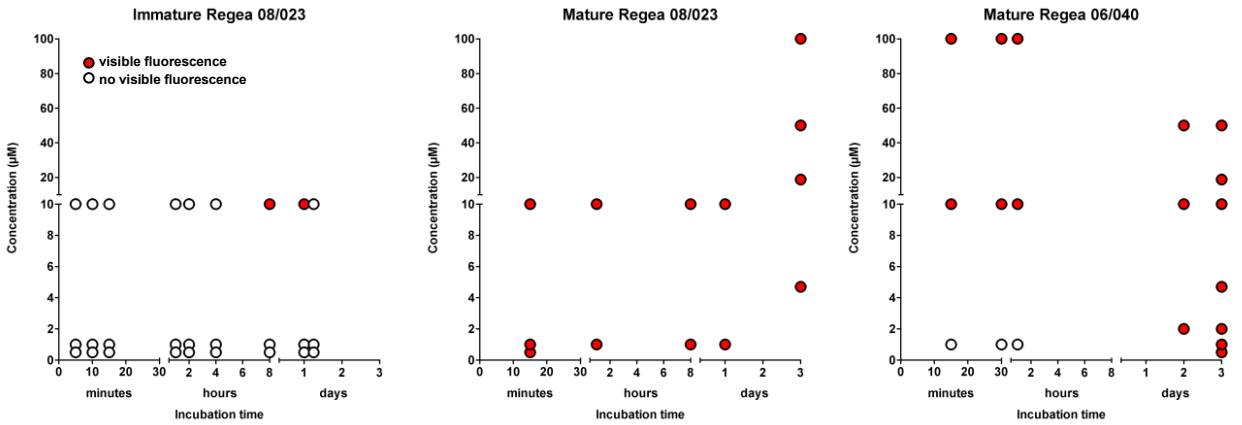

Figure 11 Achieved staining for two different hESC –lines. From the left image the effect of maturation time on staining parameters can be seen. The comparison of staining results for these two hESC –lines demonstrates the variability of labeling between different hESC –lines. For mature 08/023 2(in 1), 6(in 2) or 12(in 2) wells per staining parameters in each 5 parallel experiments, for immature 08/023 2 wells per staining parameters in 2 parallel experiments, for mature 06/040 2(in 3) or 6(in 1) wells per staining parameters in each 4 parallel experiments. Red circles represent visible fluorescence while white circles represent lack of visible fluorescence.

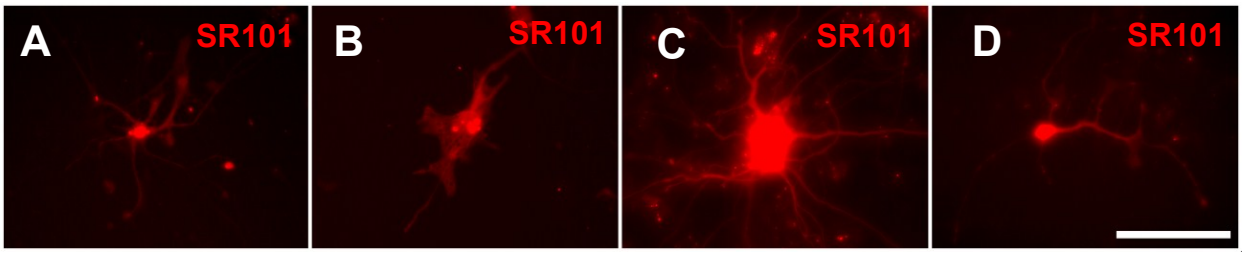

Figure 12 Presentative morphologies found in different cultures labeled with SR101. Scale bar 100µm.

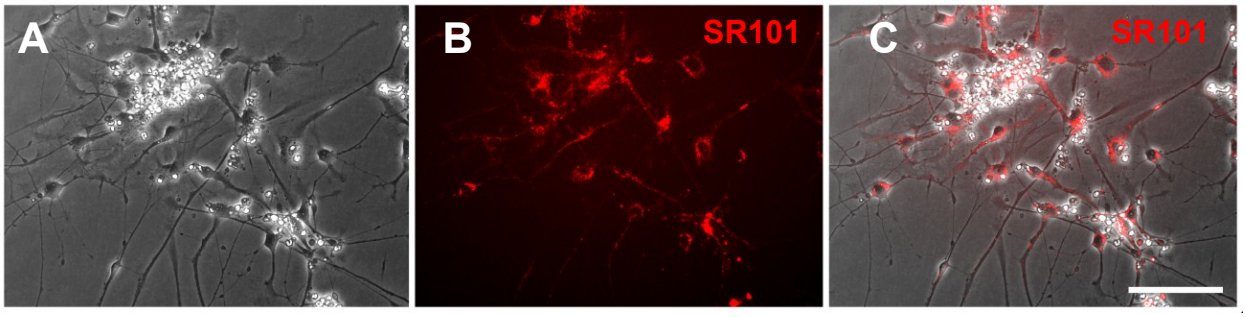

Figure 13 Granular fluorescence in SR101 labeled cells. Scale bar is 100µm.

5.1.2.2 **Behavior of SR101 fluorescence**

The cells stained with SR101 showed a series of dynamical changes in their fluorescence. At first, single cells were observed as smoothly fluorescent while the surrounding cells did not emit any light (Figure 12 A-D, Figure 14A). On the following day, only cells with granular fluorescence were found (Figure 13). This pattern of smoothly and granularly fluorescent cells repeated later in other cell cultures. The granularly fluorescent cells were always already fluorescent when observing and the density of the fluorescent granules seemed to grow as the cultures reached more mature stages. The smooth fluorescence, however, was usually initially observed on one or few SR101 labeled cells (Figure 14A), appeared during observation on several nearby surrounding cells (Figure 14B-G) and was never observed earlier than after 10 days maturation.

The appearance of fluorescence in the cultures seemed to be a dynamic process with a specific direction rather than to occur randomly (Figure 14). The morphology of the cells identified by smooth fluorescence seemed to be similar in cultures of different hESC -lines, neural differentiation and maturation times (examples in Figure 12). No further experiments were carried out to quantify the amounts of different morphologies. The smooth fluorescence did disappear from cultures, but usually reappeared in the same locations. The longest time point at which fluorescence was observed after the initial labeling was over 2.5 months.

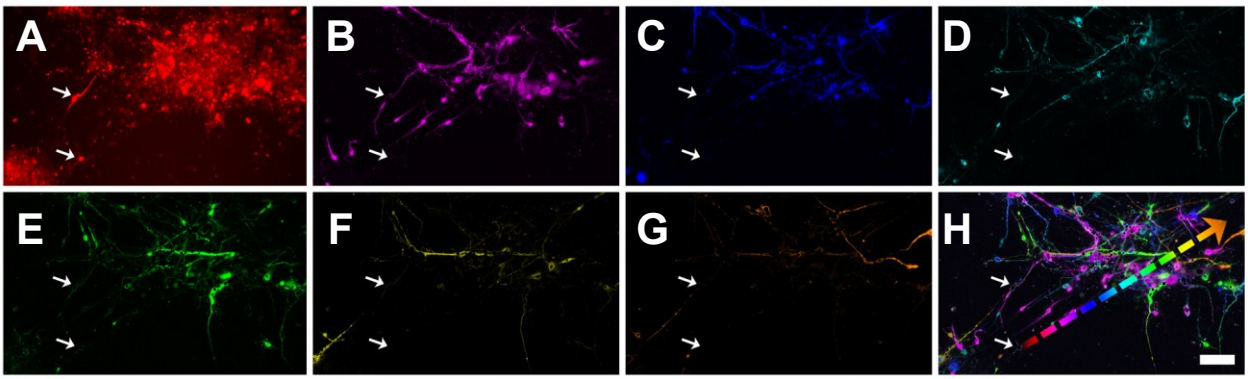

Figure 14 Cells lighting up with fluorescence. The fluorescence at the region when it was first imaged (A). Appearance of the fluorescence during the next 5 minutes (B-G). Each of the images from B-G was constructed by subtracting the previous image taken a minute earlier. This series representing the temporal change in fluorescence is combined in the image H. The gradient arrow in image H contains the pseudocoloring used in single images (B-G) from time point 0 to 5 minutes and represents the trend of fluorescence spreading in the imaged area. White arrows in images point to cells which were fluorescent during the time point zero. The scale is same for all images and the scale bar in image H is 100µm.

5.1.2.3 **Immunocytochemical staining of SR101 labeled cultures**

The cell type labeled by SR101 was studied with immunocytochemical staining. The immunocytochemical stainings were performed without permeabilization or with 0.1% saponin permeabilization. The primary antibody incubation time for overnight was used. The retainment of the fluorescence was followed up to the end of the blocking step. Up to this point, the fluorescence was retained in cells. However, during the subsequent steps of the immunocytochemical staining SR101 labeling disappeared from the cells with no permeabilization as well as from cells with saponin permeabilization. Thus, SR101 labelled cells could not be identified.

5.2. Gap junction studies

5.2.1. Studying the effects of perfusion solution on network activity

5.2.1.1 **Hepes buffered culture medium**

The cell culturing medium has a weak pH buffering capacity and during the calcium imaging it would not be sufficient to keep the pH in the physiological range. Hence, for the calcium imaging purposes, the neural growth medium was supplemented with 10mM Hepes for the first calcium imaging experiments. However, on parallel, the effect of Hepes buffered culturing media on the survival (Figure 15A) and development (Figure 15B-D) of hESC derived neural networks was studied with microelectrode arrays. 50% of the cultures survived over 20 days and two cultures of the Hepes supplemented cultures survived over

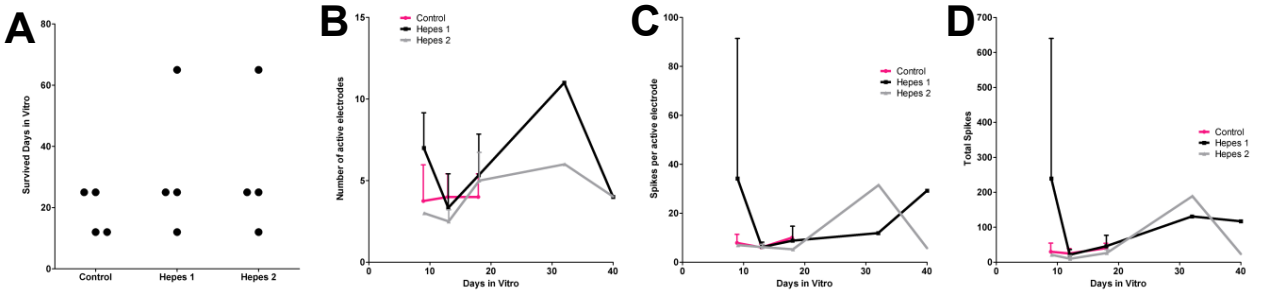

Figure 15 Comparison between control and Hepes supplemented network cultures. Comparison of the days survived between control, completely Hepes cultured (Hepes 1) and cultures changed to Hepes 9 days after plating (Hepes 2)(A). Development of the cultured networks in these three different groups with respect to active electrodes (B), spikes per electrode (C) and total spikes produced by the networks (D).

60 days. Controls died before the 3rd measurement point, and were hence followed only up to 20 days. Based on the data presented in Figure 15A, it seems that no clear difference between the survival of control cultures and Hepes supplemented cultures exists. The network activity development with respect to the amount of active electrodes, spikes per active electrodes and total spikes in cultured networks was similar between all three groups. Hence it can be stated that cultures supplemented with 10mM Hepes develop equally well compared to the control cultures.

5.2.1.2 **Ringer's solution**

As the calcium imaging measurements were planned to be performed in a Ringer's solution, the functionality of the neural networks in Ringer's solution was confirmed. Functionality was assessed by performing MEA measurements in Ringer's solution. These measurements were compared to control measurements performed with fresh medium instead of Ringer's medium. The results from measurements are presented in the Figure 16. It was observed that Ringer's solution does not cause disappearance of activity. No statistically significant differences were found between the control and Ringer's solution (two-tailed Mann Whitney test, $p > 0.05$) with respect to the number of active

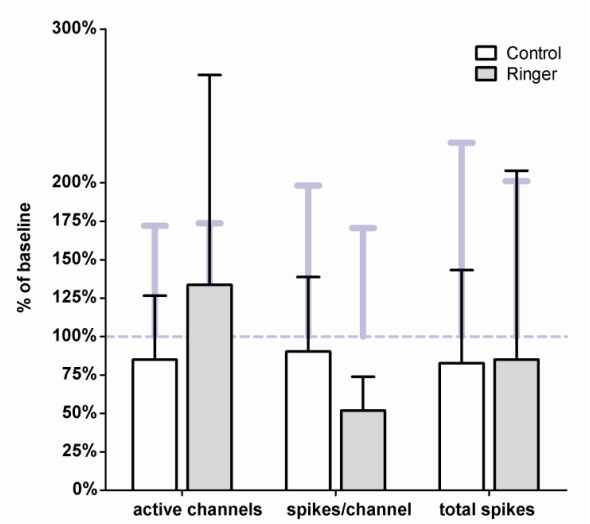

Figure 16 Measurements of network activity in fresh medium and in Ringer's solution. The blue dashed line represents the mean baseline and the blue bars above it represent the standard deviation of the baseline. White and grey bars represent the perceptual change observed in the activity after the extracellular medium was changed to fresh medium or to Ringer's solution respectively.

channels, spikes per active channels or total spikes. Based on these observations, the Ringer's solution can be used during MEA measurements without inducing any significant changes in the network function compared to the use of fresh cell culturing medium.

5.2.2. Network connections mediating the early network activity

The participation of early connections, such as gap junctions and glutamatergic synapses, in the generation of network activity recorded by MEA measurements was studied by application of pharmacological agents. In the first experiment, the changes of activity produced by gap junction blocker carbenoxolone (CBX) was studied (Figure 17A). CBX is known to have unspecific effects on the cells. However, an analogous compound, glycyrrhizic acid (GZA), reproduces these unspecific effects without blocking gap junctions. Hence, the effects of GZA on the network activity were also studied (Figure 17B). The network activity was measured at two different time points, 15 minutes and 1 hour after beginning of the incubation period. This was done in order to scale a suitable incubation time. Significant differences ($p < 0.05$) were observed between the 15 minutes CBX application and baseline but not between 1 hour CBX application and baseline (Friedman –test followed by Wilcoxon signed rank –test between baseline and both incubations). No significant differences were produced by either incubation time when GZA was applied. Thus, networks seem to exhibit gap junction mediated activity.

The effect and ability of the network to recover from the CBX application was studied in a more mature network by using a short (10 minutes) incubation time. Recovery was measured 30 minutes after washing out the CBX. Data from this experiment is presented in theFigure18A. Significant differences ($p < 0.05$) were observed between the baseline measurement and CBX application as well as between CBX application and recovery (Friedman -test followed by Wilcoxon signed rank -test between CBX application and

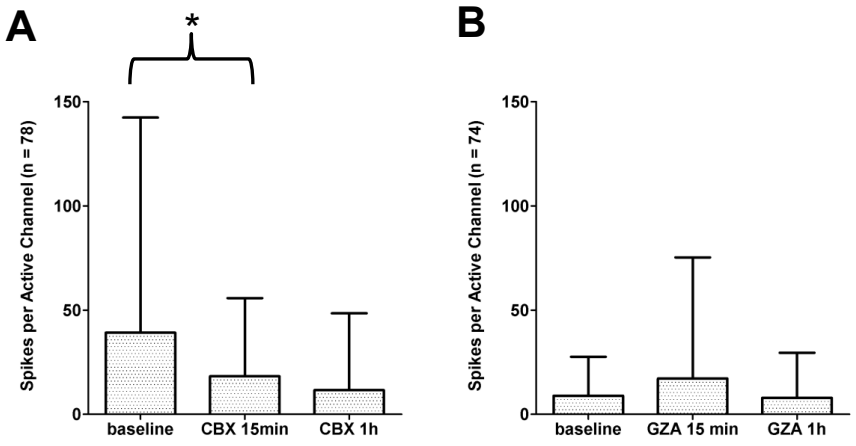

*Figure 17 The effect of gap junction blocker CBX (A) and its analog GZA (B) on the network activity. Bars represent the mean values while whiskers represent the standard deviations from these means. n is the number of active channels. *statistically significant differences.*

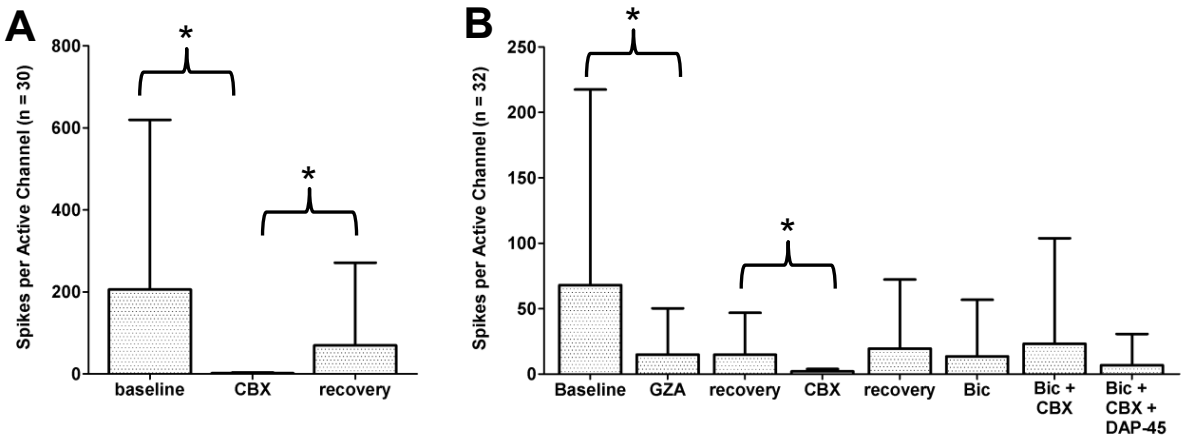

*Figure 18 The reversible effect of CBX (A) and the effect of GZA, CBX, Bic and DAP-45 of the activity of the network. Bars represent the mean values while the whiskers represent the standard deviations from this mean. n is the number of active channels.*statistically significang differences.*

baseline or recovery). From these observations it can be deduced that CBX causes a significant reversible blockage of the network activity. These observations confirm the existence of gap junctions also in more mature networks.

Next, the response of a same network to different pharmacological substances was studied (Figure 18B). First, the CBX analog GZA was applied to see the amount of unspecific effect. The drop in activity from the baseline was significant ($p < 0.05$). However, the recovery from GZA application was not significant. After measuring the recovery, CBX was applied to see the gap junction specific effect. Similar to GZA, the application of CBX caused a significant blockage of the activity with no significant recovery. The application of bicuculline (Bic) alone did not produce a significant ($p < 0.05$) change in the activity. The activity produced by Bic application was also not significantly changed by the addition of CBX. Nor was the activity significantly changed from this by the addition of DAP-45.

To conclude from the final experiment, as the GABAergic signaling of the network was blocked by Bic, the network activity was not statistically significantly changed by the blockage of gap junctions with CBX or by the blockage of NMDA receptor mediated glutamatergic signaling with DAP-45. However, the network activity was not significantly changed by the blockage of GABAergic signaling.

5.2.3. Calcium imaging

The development of gap junction coupling in hESC-derived neural networks was studied with calcium imaging. During imaging, the network under study was perfused three times with pharmacological substances. The first perfusion was performed to obtain a disinhibition by exposing the network to GABAergic signaling blocker Bic. In the second perfusion, the network activity was manipulated with gap junction blocker CBX or its non-blocking analog GZA, simultaneously with Bic disinhibition. The third perfusion was a repeat of the first perfusion. The collected imaging data was converted to calcium kinetic curves (example in Figure 19) which were classified manually. As the calcium kinetics of the cells were analyzed, it became clear that the cells showed several different response patterns to these three perfusions (Figure 20A-G, Table 3).

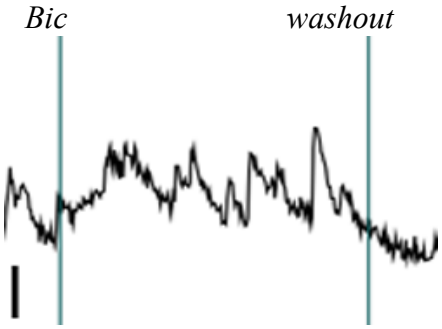

Figure 19 Example of intracellular calcium concentration change as response to Bic application. Scale bar represents a change of 50 in deltaF.

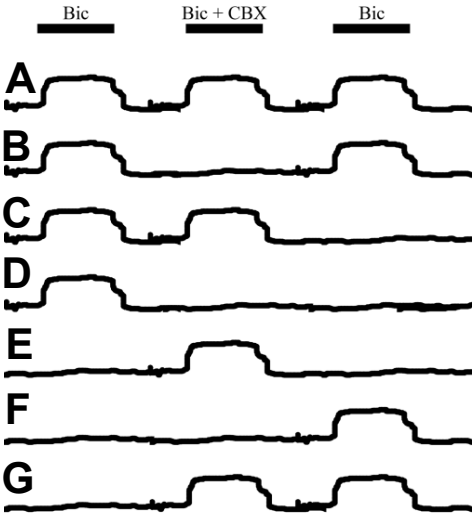

Figure 20 Different response patterns found from the networks studied. The three bars on the top represent drug applications while each line represents fluorescence kinetic for a cell belonging to each group. For each kinetic the x-axis represents time and y-axis the change in fluorescence intensity (DeltaF).

First, the cells were classified as Bic responsive or other than Bic responsive and the size of these groups were quantified. A cell was classified as a Bic responsive, if the both disinhibitions with Bic produced an intracellular calcium concentration increase (Figure 20A and B, Table 4). Thus, the other than Bic responsive cells (Figure 20C-G, Table 5) were not able to respond to both Bic applications. Some of the cells never showed calcium concentration increases (Table 3, final column).

*Table 3 Percentages of different response patterns produced to application of Bic and CBX (or GZA) for networks at different maturation staged. The patterns A-B are explained in Figure 20. * = GZA applied instead of CBX.*

Age (days)	Cell count	A (%)	B (%)	C (%)	D (%)	E (%)	F (%)	G (%)	None (%)
18	377	65	-	-	65	-	-	-	35
30	406	5	19	9	40	4	6	2	15
32	357	53	22	3	3	0	14	0	5
32*	380*	49*	-	49*	28*	0*	-	-	22*
40	496	89	1	4	0	1	0	5	0
45	412	13	3	11	17	11	3	6	36
47	334	4	0	3	15	20	5	6	47

Table 4 Percentages of Bic responsive cells with cell numbers. Two last columns represent percentages of Bic responsive cells which also showed a response during CBX+Bic application (A) or showed no response during CBX+Bic application (B).

Age (days)	Bic responsive (%)	Cell counts of Bic responsive	A (%)	B (%)
30	24	98/406	19	81
32	75	267/357	71	29
40	90	446/496	99	1
45	16	66/412	82	18
47	4	14/334	100	0

Table 5 Percentages of other than Bic responsive cells with cell numbers. Six final columns represent percentages of other than Bic responsive cells belonging to each category (C-G, None).

Age (days)	Other than Bic responsive (%)	Cell counts of other than Bic responsive	C (%)	D (%)	E (%)	F (%)	G (%)	None (%)
30	76	308/406	11	52	5	8	3	20
32	25	90/357	11	13	0	56	0	20
40	10	50/496	38	2	8	0	48	4
45	84	346/412	13	20	13	4	8	43
47	96	320/334	3	15	21	5	6	49

The proportion of Bic responsive versus other than Bic responsive cells during network maturation is depicted in Figure 21. The numeric values for these two groups can be found from the Table 4 and Table 5. A trend with first increasing and then decreasing phase was observed for the proportion of Bic responsive cells. The maximum of proportion of GABAergic signaling inhibition activated cells was observed to occur at 40 days maturation time (Figure 21). After this point, the proportion of Bic responsive cells was seen to decrease rapidly. The trend of proportion of Bic responsive cells would then indicate an initial increase of GABAergic inhibition after 30 days network maturation followed by a rapid decrease in GABAergic inhibition.

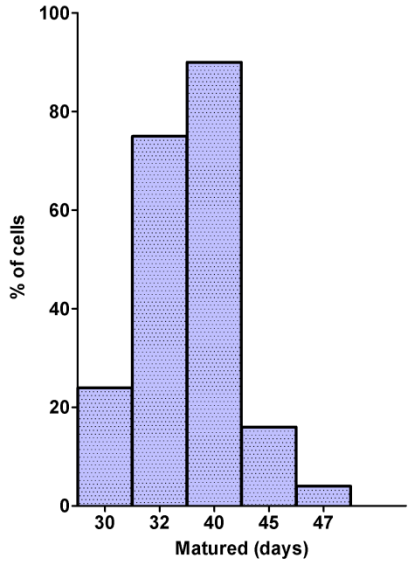

Figure 21 The percentage of Bic responsive cells from all cells with different network maturation times. The cells not belonging to Bic responsive group belonged to other than Bic responsive group and thus this group constitutes as the rest of the percentage.

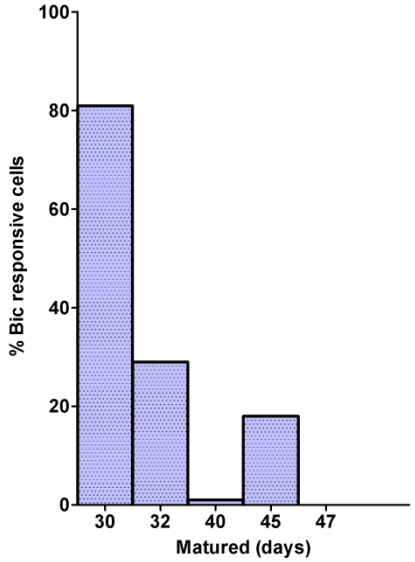

Figure 22 Percentages of the B group from Bic responsive cells. Rest of the Bic responsive cells belonged to the A group.

Next, the gap junctional coupling during network maturation was quantified by counting the amount of Bic responsive cells which response to disinhibition was blocked by the gap junction blocker CBX (Figure 20B, Table 4, 4th column). A clear decreasing trend was observed for the amount of Bic responsive cells affected by the gap junction blockage Figure 22). The proportion of these cells decreased from the initial 81% at the earliest maturation point studied, to final 0% at the latest maturation point studied. Thus, it seems that, the amount of gap junction coupled cells decreases during the *in vitro* network maturation from very high to non-existent amounts.

In addition, the other than Bic responsive cells, showing inconsistent activation by disinhibition, were further classified and the proportions of formed classes were quantified with respect to the amount of other than Bic responsive cells (Table 5, Figure 23).

Cells of the group C (Figure 23) were activated by the first Bic and the second Bic+CBX application, but not by the final Bic application. The proportion of cells in this group was relatively low in networks of all studied maturation stages, except for the cells studied at 40th day of maturation.

The group D (Figure 23) consisted of cells which were activated only by the first inhibition of the GABAergic signaling of the network. This group of cells was largest in the most immature networks studied and was roughly of the same size in the more mature networks.

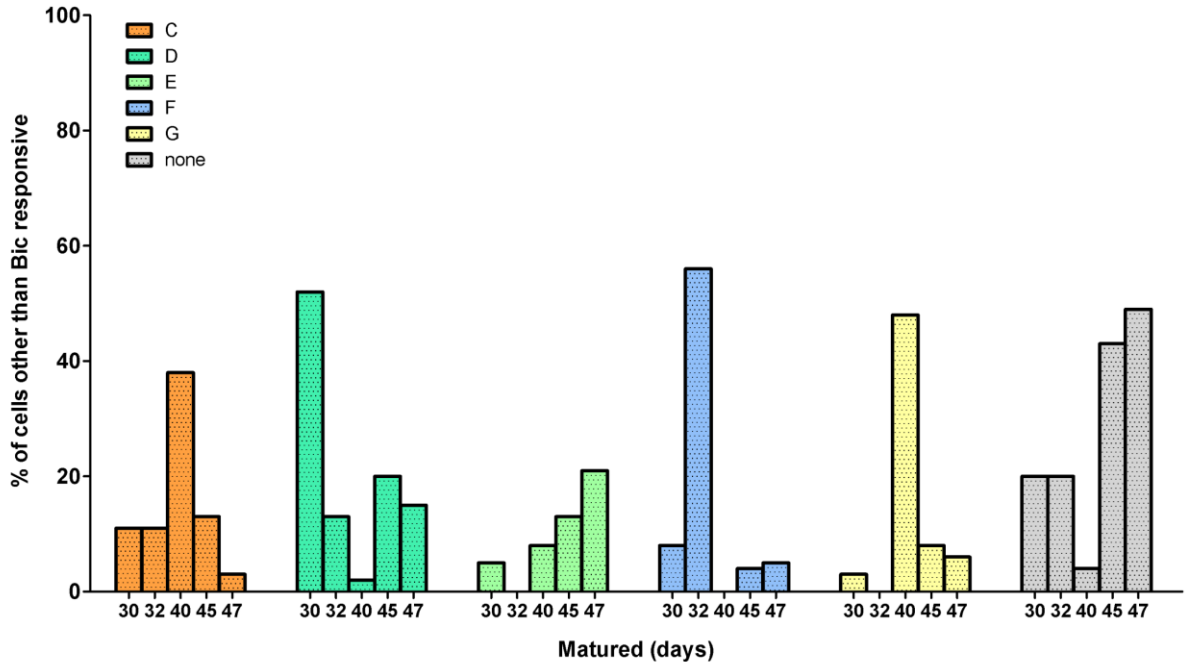

Figure 23 Subgroups of other than Bic responsive cells as proportions of other than Bic responsive cells. Each group is arranged to describe the development of proportion of other than Bic responsive cells in that particular group.

Cells of the group E (Figure 23) showed intracellular calcium level rises only to the simultaneous blockage of GABAergic and gap junction mediated signaling. The proportion of cells in this group was relatively low in all studied network maturation stages, however, a slight increase was observed during the maturation of the network.

The group F (Figure 23) was characterized by a response to only the final application of the GABAergic signaling blocker Bic. The proportion of cells in this group was very low in all network maturation stages with the exception of the cells measured during 32th day of maturation.

The group G (Figure 23) consisted of cells responding to the simultaneous Bic and CBX application and to the final Bic application, however, showing no response to the first Bic application. Similar to the group C, the proportion of cells belonging to this group was relatively low in all networks studied with the exception of the networks matured for 40 days.

The proportion of cells producing no response (Figure 23) to any of the three GABAergic antagonist Bic containing perfusion, on the other hand, was substantial in the two most mature network stages studied, very low in the 40 days matured networks and in between these extremes in the two most immature network stages studied. This observation

indicates a decreasing ability of the GABAergic signaling inhibition to induce activity in the more mature networks.

6. Discussion

6.1. CellTracker in labeling live cells

6.1.1. CT optimization

Based on the wide variety of parameters tested, the 10μM CT in culture medium with 72 hour incubation time is the best option to produce a long term hESC derived neural cell labeling. These labeling parameters enable cell visualization at least up to 4 weeks. The long incubation time needed to achieve long retainment of the dye could be due to more CT entering the cells and becoming attached to intracellular molecules compared to shorter incubation time. While higher concentrations with lower incubation times did produce lengthening of the retainment period, this could be worse option because of the load caused to intracellular esterases.

Labeling with CT by using the optimized parameters was observed to produce a tint background labeling. This is most likely due to a reaction between the dye and laminin coating as replated prelabeled cell cultures had less background than their prelabeled controls. Thus, the reactivity of CT chromethyl moieties with protein thiols (Molecular Probes® Handbook, Section 14.2) should be taken into account when considering staining cell cultures containing biomaterials as the biomaterials containing thiol groups might also become labeled. This becomes even more important if the labeled cells and material were transplanted because the fluorescence could be from both cells and material or only from material alone if the cells died.

In addition to coating materials, CT might also react with medium components and more efficient staining might be produced if the label was diluted to protein free PBS rather than to cell culture medium. On the other hand, the use of medium could allow better viability during long incubation times while more efficient loading and labeling might cause load to intracellular esterases. It could also be possible that short and efficient labeling might label a smaller population of biomolecules very efficiently while the long incubation would allow labeling of a larger population of biomolecules.

In literature, the labeling parameters used to label neural lineage cell cultures tended to follow those recommended by the Molecular Probes. For example: 20μM for 30 minutes (McMahon and McDermott, 2006), 5μM for 60 minutes (Petterson et al., 2010) and 10μM for 30 minutes (Markiewicz et al., 2011). The observations about the CT lasting varied as

CT labeled radial glial cells were reported to be observable up to 20 days (McMahon and McDermott, 2006) while CT labeled olfactory ensheathing glial cells lost their fluorescence in under 14 days (Petterson et al., 2010). However, the parameters used by Petterson and colleagues (2010), McMahon and McDermott (2006), and Markiewicz and colleagues (2011) were not optimized for the cells used.

6.1.2. Effect on viability and proliferation

CT did not clearly decrease or increase the viability of hESC derived neural cells. No statistically significant difference was observed between CT stained and control cultures. However, the proportion of dead cells in labeled cultures seemed to be larger after longer period from labeling (15 days). Based on this observation, it could be possible that CT induces a decrease in the viability during long term. Hence the effect of CT on cell viability should be also studied at later time points up to 4 week time, during which the CT labeled cells are visible. It is possible that cells were more easily counted as dead than as alive due to more clear visualization of dead cells from groups of cells growing tightly packed. On the other hand, this error would exist for both control and CT labeled cultures and hence it should play no role when comparing proportions of dead cells between these two groups. No literature assessing the viability effect of CT was found.

CT did not affect the proliferation of hESC derived neural cells. During experiments no trend with respect to post labeling period length was observed and the experiment was repeated several times. Some error might have been caused by the calculations as some of the nuclei were lightly stained while others were very brightly stained. However, as with viability experiments, the comparison was done between proportions of proliferating cells in control and CT stained cultures and both groups have this same error factor. Contradictory, CT has previously been described to reduce the proliferation rate of labeled olfactory ensheathing cells (Petterson et al., 2010). The labeling performed by Petterson and colleagues (2010) was done with a lower CT concentration and the incubation time was shorter than the incubation time used in this study. Because these gentler labeling parameters affected proliferation, it is possible that such effects are elicited cell type dependently.

6.1.3. Optimizing immuno cytochemistry for fluorescent dyes

Performing an immunostaining with 1% saponin permeabilization and 3 hour primary antibody incubation time could be used for cell labeled with fluorescent dyes. An immunostaining protocol with these modifications produces specific and clearly

visualizable immunostaining and is more likely to allow the retention of fluorescent dyes in cells. The use of cholesterol-specific detergent, such as saponin, instead of Triton-X has been previously described to allow the retainment of a membrane dye during immunohistochemistry (Matsubayashi et al., 2008). However, as the 3 hour primary incubation time was the shortest studied even briefer incubation times could be tried out to minimize dye diffusion. Unfortunately, this immunocytochemistry was not studied with DiD or SR101 labeled cells which more easily lose their fluorescent label compared to CT. On the other hand, all permeabilization and primary incubation parameters studied allowed the retention of CT and clear immunolabeling.

6.1.4. Type of cells labeled by CT

CT seems to label all the hESC derived neural cells. However, the percentage of CT labeled cells was observed not to reach 100%. This is most likely due to the more easy visualization of DAPI stained nuclei compared to CT stained cell body from groups of tightly packed cells. These observations are in line with the previous work describing successful CT labeling of human cord blood-derived neural stem cells differentiated in to neurons, astrocytes, oligodendrocytes and microglia (Markiewicz et al., 2011) as well as olfactory ensheathing (Petterson et al., 2010) and radial glial cells (McMahon and McDermott, 2006).

6.1.5. Using CT in cocultures with DiD

CT is suitable for experiments where labeled cells need to be replated as well as for experiments involving co-culturing with DiD labeled cells. CT could also possibly be used to study interactions between co-cultured cells. CT can be argued to be suitable for replating due to the observed retainment of the dye in cells after replating. The effect of replating on the maximal visualization time, however, was not studied. During the co-culturing of CT and DiD labeled cells some of the cells had both dyes in them. However, cells which were originally labeled with CT or DiD could be separated as cells which had taken up CT or DiD from other cells could be separated from those which were originally labeled with CT or DiD. The co-localization of CT and DiD to same cells could be due to cells engulfing parts of each other during close cell-cell interactions.

hESC derived neuronal cells labeled with CT and DiD are able to form active connections giving rise to a functional neural network. MEA measurement used to study the development of co-cultured networks containing both CT and DiD labeled neurons allow the observation of the development of the network activity. This method, however, does

not enable the direct study of synapses or detailed electrophysiological features of single cells. Hence, the network activity measured by MEA can be argued to demonstrate that separately CT and DiD labeled co-cultured neural cells are able fire action potentials and are able to form a functional network. Unfortunately, based on this method, nothing can be concluded about the formation of synapses between the two differently labeled cell populations or about supple effects of these dyes on the electrophysiological properties of cells. These aspects could be studied in the future by utilizing patch clamp or calcium imaging methods and immunocytochemical staining against synaptic structures. No studies describing the use of dual fluorescent dye labeled neural cells in co-cultures were found.

6.2. Sulforhodamine 101 in labeling live cells

6.2.1. SR101 optimization

The optimal parameters for labeling cells with SR101 are 10μM dye in medium during 8 hours incubation time. The above mentioned parameters can be argued to be optimal as they were the lowest concentration and shortest incubation time always producing labeling. Using lowest concentration and shortest incubation time possible is desired in order to affect the cell physiology as little as possible. Much shorter incubation time were found to be used previously (Nimmerjahn et al., 2004; Kafitz et al., 2008).

During the SR101 labeling parameter optimization, the labeling was observed to depend on the cell line used as well as on the time the cells were allowed to mature after plating them for adherent culturing. This dependency was seen as more mature cells were labeled with lower dye concentrations and with shorter incubation times than more immature cells. In addition, a culture where cells were not labeled with certain suboptimal parameters was successfully labeled by performing the staining with these same parameters few days after the first attempt. Hence, I would like to suggest, that as SR101 uptake is thought to occur via an active astrocyte uptake mechanism (Kafitz et al., 2008), this cell line and maturation dependency could reflect the maturation of this active uptake mechanism.

If the SR101 labeling would reflect the maturation of efficiency of an active mechanism and if this mechanism was astrocyte specific, SR101 labeling could be used to study the maturation of astrocytes or the labeling parameters could be tweaked to label a population of astrocytes which had reached a certain stage of maturity. The connection between SR101 labeling and the astrocyte maturity would hence be an interesting aspect to study.

Another aspect which should be assessed is the cytotoxicity of the SR101 which was not done in this project.

6.2.2. Behavior of SR101

The labeling produced by SR101 was observed to have a dynamic nature. Often the SR101 labeling was observed to produce a smooth labeling spreading from one cell to other cells located in close distance. This spreading of fluorescence was relatively slow, seemed to have a direction and was confined to a part of the cell culture. No descriptions of similar phenomena with SR101 were found from the literature. During follow up after the appearance of the fluorescence, the smooth fluorescence developed a granular appearance. During further follow up the fluorescence disappeared from the cells, but was also able to reappear without relabeling in a similar matter as it was first observed to appear. The reappearance of the fluorescence has not been described before.

In literature, the transition from a smooth fluorescence into a granular fluorescence has been suggested to occur due to compartmentalization of the dye into mitochondria (Kafitz et al., 2008). This could be studied by labeling the mitochondria and studying co-localization or by separating the mitochondria by centrifugation and observing whether the fluorescence was also separated or by studying the effects of drugs affecting mitochondria function on the behavior of the SR101 fluorescence. However, this does not explain the phase of complete disappearance of the fluorescence. One possibility, on the other hand, could be the quenching of fluorescence in the mitochondria due to high fluorophore interactions.

If the granularization and disappearance of the fluorescence of the SR101 labeled cells would be due to compartmentalization into mitochondria, the reappearance of the fluorescence could then be argued to be caused by the release of SR101 from the mitochondria. Such release could possibly be introduced by the activation of the mitochondria. Following this line of thought, the somewhat organized spreading of the dye could be thought to depend on an intercellular communication mechanism causing a mitochondrial activation ultimately leading to the release of the dye back to cytoplasm. In literature, spreading of the activity or injected dye into a defined local cellular network has been described to occur for both, neurons (Yuste et al., 1995; Kandler, 1998) and astrocytes (Nimmerjahn et al., 2004; Kafitz et al., 2008). The dependence of the fluorescence spreading on cellular activation could, in the future, be assessed by calcium

imaging while the participation of gap junctions could be studied with dye injections similar to those described in the literature.

6.2.3. Type of cells labeled by SR101

SR101 did not label all the cells in the hESC derived neural cell cultures. SR101 could be argued to produce an astrocyte specific labeling based on the observations that the cells labeled by SR101 did not resemble the morphology of neurons, flat epithelial like cells or oligodendrocytes. In addition, some of the clearly distinct morphologies observed for SR101 labeled cells were also observed to be represented in GFAP positive cell population labeled during the optimization of the immunocytochemical staining protocol for fluorescent dyes. However, the correctness of these conclusions should be ensured with some immunocytochemical stainings.

Immunocytochemistry was performed for SR101 labeled cells but the label was lost from the cells. In literature, SR101 was claimed to disappear during the fixation of cells (Nimmerjahn et al., 2004; Kafitz et al., 2008). This, however, was not observed as the cells were imaged after fixing. During experiments, the SR101 was observed to disappear from the cells only after the primary antibody incubation. However, the immunocytochemistry was not performed with 1% saponin and 3h primary antibody incubation which could allow the retainment of the dye during immunocytochemistry. As an alternative, if no suitable immunocytochemical staining protocol is found for the cells, expression of a fluorescent protein under astrocyte specific promoter could be used to ensure that the cells labeled by SR101 truly are astrocytes.

6.3. Measuring with MEAs from networks in different extracellular solutions

6.3.1. Using Hepes buffering in culture medium

The development of activity in hESC derived neural networks is not inhibited by Hepes buffered culture medium. However, the number of networks studied in this experiment was so low that supple differences in network activity development could not have been observed. Another possibily to observe supple effects in network activity would be to compare recorded spikes forms. This, however, was not done due to the lack of suitable automated analysis needed in order to analyze the huge amounts of spike forms recorded.

The networks cultured in Hepes buffered medium survived longer than the control cultures. This could indicate that Hepes buffering promotes network survival during experiments

with repeated measurements. However, due to the small number of networks studied, these kinds of conclusions are not reliable. Hepes buffering could promote the survival by resisting the pH change taking place during the measurements which are done at normal room atmosphere without any perfusion system.

6.3.2. Using Ringer's solution during measurements

The use of Ringer's solution during MEA measurements does not cause disappearance of the activity hESC derived neural network activity. Instead, the activity of the hESC derived neural network was changed as the number of active sites within the network grew with a small drop in overall activity. This caused a clear drop in the activity detected per active site. In the fresh medium control the number of active sites was slightly decreased with a small drop in overall activity. The activity per active network location, however, remained almost unchanged. No statistically significant results were revealed. This difference most likely arose from the changes caused by the difference in ionic compositions between Ringer's solution and the culture medium.

As different labs use different culture mediums and as the ionic compositions of the components of culture mediums can vary a solution of known ionic compositions should be used when making network measurements. The effects could be even clearer, if a pharmacological test was compared between a network in different culture mediums and a network in solution of known ionic composition. In literature, Ringer's solution has been used on MEA (Illes et al., 2007). Different ionic concentrations have also been studied (Canepari et al., 1997), but the differences between culture medium and Ringer's solution have not previously been assessed.

6.4. Mechanisms mediating network activity studied with MEA

Gap junctions, glutamatergic and GABAergic signaling mechanisms are functional in the hESC derived neural networks. In addition, the spontaneous activity of these networks is almost completely dependent on gap junctional communication. The participation of gap junctions in the activity measured by MEA was studied by comparing the effect of dirty gap junctions blocker CBX and its control analog GZA, which should replicate the unspecific effects of CBX (Rouach et al., 2003). CBX had a reversible effect unlike GZA. Due to these observations about the differences between CBX and GZA effects it can be argued that the CBX produced effect should result from the reversible and specific blockage of the gap junctions. The network activity can be argued to be partly mediated by gap junctions as the effect of CBX on the network activity was clearly larger than that of GZA. CBX

addition almost completely blocked the network activity indicating that gap junctions have large role.

The addition of $GABA_A$ receptor blocker bicuculline alone did not have clear effects and from that one might conclude that no GABAergic mechanisms participated in the generation of the network activity. However, the lack of effect might arise from the short incubation time of bicuculline and its effects could be reflected on the results gathered from the next measurement. The effect of CBX was diminished by the presence of bicuculline, however, as the full effect of bicuculline might not have been measured when performing measurement from networks which were applied bicuculline alone it could be that bicuculline raised the activity and some of this was blocked by CBX resulting in seemingly less blockage than during previous application of CBX.

NMDA receptor mediated glutamatergic signaling mechanisms were observed to exist in the hESC derived neural networks and they mediated the activity caused by the inhibition of $GABA_A$ receptors and gap junctions. This can be argued as the activity which was generated by bicuculline application and was not diminished by CBX application was diminished by NMDA receptor blockage. The participation of NMDA receptors in the hESC derived neural network activity mediation has also been previously shown (Heikkilä et al., 2009).

These observations are in line with previous information obtained from the *in vivo* formed neural networks in which gap junctions have been shown to participate in the mediation of early spontaneous network activity (Rouach et al., 2003; Dupont et al., 2006; Khazipov and Luhmann, 2006; Sun and Luhmann, 2007; Sun et al., 2008; Takayama et al., 2009; Peinado, 2011). Other work studying the participation of gap junctions to network activity mediation in ESC-derived networks was not found. Similarly, also the participation of other synaptic signaling mechanisms has been previously shown to occur in *in vivo* formed networks (Kanold and Luhmann, 2010).

6.5. Calcium imaging

In this study, the ESC derived neural networks seemed to capture some of the stages typically appearing during the network development of non-human primary cell cultures and *in vivo* networks (Yuste et al., 1995; Kandler, 1998; Khazipov and Luhmann, 2006; Baltz et al., 2010; Peinado, 2011). These aspects include the change on the role of GABAergic signaling in the network activity and the decrease of the gap junctional coupling. These observations rise the question of how much more similarities to the *in vivo*

developing network are captured in the cellular network of the *in vitro* differentiated hESCs.

6.5.1. Bicuculline responsive cells

The inhibition by GABA signaling first increases and then decreases during the development of hESC derived neural networks. The amount of GABAergic inhibition can be thought to reflect the amount of GABAergic inhibitory synapses which in this light would first increase and later become eliminated. This conclusion is based on the observation of the growth of the proportion of cells responding with an intracellular calcium level rise to the $GABA_A$ receptor blocker application. A change in the role of GABAergic signaling during the maturation of *in vitro* grown network has previously been described to take place in fetal cortex derived primary cell cultures (Baltz et al., 2010). According to Baltz and colleagues (2010), the initial network activity occurs independently of GABA while the later network activity is controlled by an increasing amount of GABAergic signaling.

It is important to acknowledge that the calcium level rises accepted during the analysis as responsiveness were not limited to oscillatory rises but any intracellular calcium concentration rise caused by the perfused substance was included. Only the oscillatory calcium level rises have been previously associated with bicuculline induced disinhibition (Kato-Negishi et al., 2003; Rouach et al., 2003). In addition, due to perfusion problems encountered during the series of experiments, cells from one time point generally consist of cells measured within one field of view. Hence, the errors affecting the field of view would be replicated to all cells studied at that time point. On the other hand, as the change in responsiveness to the $GABA_A$ receptor blocker formed a trend, it could be argued that the results were not suffering from this kind of error. However, the study should be repeated with more parallels at the same time point as well as with additional time points in order to gain more information about the timing and the rate of changes in the GABAergic signaling of the maturing networks. Addition of a GABA application to the experiments would allow even more detailed study of the function of the GABAergic system in the maturing networks. For example, the developmental change of GABA from excitatory to inhibitory could be studied if the effect of both GABA agonist and antagonist was observed.

6.5.2. Gap junction coupled cells

The role of gap junctional coupling as mediator of the network activity was observed to decrease during the maturation of hESC derived neural networks. This was seen as a

decreasing trend of the amount of cells in which bicuculline induced intracellular calcium level rise was reversibly prevented by blocking gap junctions.

As discussed above with respect to bicuculline responsive cells, more parallels and more timepoints should have been used in this set of experiments. In addition, the specificity of CBX should have been ensured for each time point during maturation by GZA application to confirm that the network or its component cells do not acquire any features which would allow the unspecific action of the gap junction blocker. Also, as the methodology used is highly indirect, it would be fruitful to carry out additional repeats with more conventional methods, such as dye spreading via gap junctions.

In literature, similar observations about the sharp decrease of gap junctional coupling during the maturation of neural network have been reported to occur *in vitro* and *in vivo* (Dupont et al., 2006; Khazipov and Luhmann, 2006; Peinado, 2011). Clear domains of simultaneously active neurons, similar to those described *in vivo* (Yuste et al., 1995; Kandler, 1998; Dupont et al., 2006; Kanold and Luhmann, 2010; Peinado, 2011), were not observed during imaging. However, no detailed analyses were performed to study this aspect.

6.5.3. Other than bicuculline responsive cells and methodological considerations

In addition to the already described results several unexpected patterns of responses were found. From the gathered data it is hard to conclude whether these patterns are associated with some biologically relevant phenomena or are merely artifacts of the calcium imaging.

There are at least three possible explanations for the observed patterns. One of these explanation is the possible errors arising from discontinuous recordings belonging to the same experiment. This would cause error to all cells within the same field of view if the ratio of the base line changed during the breaks in recordings. Such changes of ratio would arise from the change of liquid level due to unstable perfusion or from uneven exposure time recalibration. The change of ratio in baseline would cause a change in the deltaF values as these are calculated as percentage of the baseline. The existence of this kind of error would be revealed by several parallel experiments performed at the same time point.

Another possible explanation is rise of intracellular calcium level due to the spontaneous activity of the cell or network, rather than due to application of bicuculline. The spontaneous activity could have affected the measurements i.e. by causing bicuculline independent rises of calcium level during disinhibition and by causing inability of the cell to respond to disinhibition due to refractory period of the earlier activity. This is quite possible as spontaneous activity was seen to occur during periods when no drugs were applies.

The third possible explanation would be the amount and change of excitatory activity in the network. The blockage of GABAergic signaling causes disinhibition, but this alone might not be enough to cause the cell to fire and additional exitatory input to the cell could be required. Differences in this excitatory activity along the experiment would then be able to produce the unexpected patterns. The change in the exitatory activity between different maturation points studied could then also explain the maturation point dependent changes in the proportions of different unexpected patterns.

7. Conclusions

Two different dyes were optimized for long-term labeling of hESC-derived neurons. The optimal parameters for CT were 10μM concentration with 72 hour incubation time and for SR101 10μM concentration with 8 hour incubation time. CT was able to label the cells up to 4 weeks, did not affect cell proliferation or viability and labeled all cell types. CT was found to be suitable for co-culturing studies. SR101 labeling, on the other hand, was observed to depend on cell line and maturation stage. SR101 labeling was also observed to behave dynamically and the cells labeled by SR101 were concluded to be astrocytes. However, this could not be confirmed by immunocytochemistry due to SR101 disappearance.

The role of gap junctions in the neural network activity of maturing hESC-derived networks was characterized in an extracellular solution which suitability was ensured. Gap junctions were found to mediate the spontaneous network activity together with glutamatergic and GABAergic signaling. In addition, the maturing networks were found to exhibit *in vivo* like changes in gap junction coupling. However, these findings should be more carefully studied in future experiments.

8. References

Alexander, J.M. and Bruneau, B.G. (2010). Lessons for cardiac regeneration and repair through development. Trends in molecular medicine 16(9), 426-434.

Allène, C., and Cossart, R. (2010). Early NMDA receptor-driven waves of activity in the developing neocortex: physiological or pathological network oscillations? The Journal of physiology, 588(1), 83-91.

Allène, C., Cattani, A., Ackman, J. B., Bonifazi, P., Aniksztejn, L., Ben-Ari, Y., and Cossart, R. (2008). Sequential generation of two distinct synapse-driven network patterns in developing neocortex. The Journal of neuroscience : the official journal of the Society for Neuroscience, 28(48), 12851-63.

Baltz, T., de Lima, A. D., and Voigt, T. (2010). Contribution of GABAergic interneurons to the development of spontaneous activity patterns in cultured neocortical networks. Frontiers in cellular neuroscience, 4(June), 15.

Ban, J., Bonifazi, P., Pinato, G., Broccard, F. D., Studer, L., Torre, V., and Ruaro, M. E. (2007). Embryonic stem cell-derived neurons form functional networks in vitro. Stem cells (Dayton, Ohio), 25(3), 738-49.

Burns, S. P., Xing, D., and Shapley, R. M. (2010). Comparisons of the dynamics of local field potential and multiunit activity signals in macaque visual cortex. The Journal of neuroscience : the official journal of the Society for Neuroscience, 30(41), 13739-49.

Canepari, M., Bove, M., Maeda, E., Cappello, M., and Kawana, a. (1997). Experimental analysis of neuronal dynamics in cultured cortical networks and transitions between different patterns of activity. Biological cybernetics, 77(2), 153-62.

Chiappalone, M., Bove, M., Vato, A., Tedesco, M., and Martinoia, S. (2006). Dissociated cortical networks show spontaneously correlated activity patterns during in vitro development. Brain research, 1093(1), 41-53.

Claverol-Tinture, E., and Pine, J. (2002). Extracellular potentials in low-density dissociated neuronal cultures. Journal of neuroscience methods, 117(1), 13-21.

de Lima, A. D., Gieseler, A., and Voigt, T. (2008). Relationship between GABAergic interneurons migration and early neocortical network activity. Developmental neurobiology, 69(2-3), 105-23.

Colonnese, M. T., and Khazipov, R. (2010). “Slow activity transients” in infant rat visual cortex: a spreading synchronous oscillation patterned by retinal waves. The Journal of neuroscience : the official journal of the Society for Neuroscience, 30(12), 4325-37.

Dupont, E., Hanganu, I. L., Kilb, W., Hirsch, S., and Luhmann, H. J. (2006). Rapid developmental switch in the mechanisms driving early cortical columnar networks. Nature, 439(7072), 79-83.

Froemke, R. C., Kumar, V. S., Czkwianianc, P., and Yuste, R. (2002). Analysis of multineuronal activation patterns from calcium-imaging experiments in brain slices. Trends in cardiovascular medicine, 12(6), 247-52.

Gaspard, N., Bouschet, T., Hourez, R., Dimidschstein, J., Naeije, G., van den Ameele, J., Espuny-Camacho, I., et al. (2008). An intrinsic mechanism of corticogenesis from embryonic stem cells. Nature, 455(7211), 351-7.

Germain, N., Banda, E., and Grabel, L. (2010). Embryonic stem cell neurogenesis and neural specification. Journal of cellular biochemistry, 111(3), 535-42.

Grynkiewicz, G., Poenie, M., and Tsien, R. Y. (1985). A new generation of Ca2+ indicators with greatly improved fluorescence properties. The Journal of biological chemistry, 260(6), 3440-50.

Gullo, F., Mazzetti, S., Maffezzoli, A., Dossi, E., Lecchi, M., Amadeo, A., Krajewski, J., et al. (2010). Orchestration of “presto” and “largo” synchrony in up-down activity of cortical networks. Frontiers in neural circuits, 4(April), 11.

Görtz, P., Fleischer, W., Rosenbaum, C., Otto, F., and Siebler, M. (2004). Neuronal network properties of human teratocarcinoma cell line-derived neurons. Brain research, 1018(1), 18-25.

Heikkilä, T. J., Ylä-Outinen, L., Tanskanen, J. M. a, Lappalainen, R. S., Skottman, H., Suuronen, R., Mikkonen, J. E., et al. (2009). Human embryonic stem cell-derived neuronal cells form spontaneously active neuronal networks in vitro. Experimental neurology, 218(1), 109-16.

Hogberg, H. T., Sobanski, T., Novellino, A., Whelan, M., Weiss, D. G., and Bal-Price, A. K. (2011). Application of micro-electrode arrays (MEAs) as an emerging technology for developmental neurotoxicity: evaluation of domoic acid-induced effects in primary cultures of rat cortical neurons. Neurotoxicology, 32(1), 158-68.

Hovatta, O. (2003). A culture system using human foreskin fibroblasts as feeder cells allows production of human embryonic stem cells. Human Reproduction, 18(7), 1404-1409.

Illes, S., Fleischer, W., Siebler, M., Hartung, H.-P., and Dihné, M. (2007). Development and pharmacological modulation of embryonic stem cell-derived neuronal network activity. Experimental neurology, 207(1), 171-6. doi:10.1016/j.expneurol.2007.05.020

Illes, S., Theiss, S., Hartung, H.-P., Siebler, M., and Dihné, M. (2009). Niche-dependent development of functional neuronal networks from embryonic stem cell-derived neural populations. BMC neuroscience, 10, 93.

Inzunza, J, Sahlén, S., Holmberg, K., Strömberg, a-M., Teerijoki, H., Blennow, E., Hovatta, O., et al. (2004). Comparative genomic hybridization and karyotyping of human embryonic stem cells reveals the occurrence of an isodicentric X chromosome after long-term cultivation. Molecular human reproduction, 10(6), 461-6.

Inzunza, José, Gertow, K., Strömberg, M. a, Matilainen, E., Blennow, E., Skottman, H., Wolbank, S., et al. (2005). Derivation of human embryonic stem cell lines in serum replacement medium using postnatal human fibroblasts as feeder cells. Stem cells (Dayton, Ohio), 23(4), 544-9.

Jäderstad, J., Jaderstad M., Li J. et al. (2010). Communication via gap junctions underlies early functional and beneficial interactions between grafted neural stem cells and the host. Proceedings of the National Academy of Sciences of the United States of America 107, 5184-9.

Kafitz, K. W., Meier, S. D., Stephan, J., and Rose, C. R. (2008). Developmental profile and properties of sulforhodamine 101--Labeled glial cells in acute brain slices of rat hippocampus. Journal of neuroscience methods, 169(1), 84-92.

Kamioka, H., Maeda, E., Jimbo, Y., Robinson, H. P., and Kawana, a. (1996). Spontaneous periodic synchronized bursting during formation of mature patterns of connections in cortical cultures. Neuroscience letters, 206(2-3), 109-12.

Kandler, K. (1997). Coordination of neuronal activity by gap junctions in the developing neocortex. Seminars in cell and developmental biology, 8(1), 43-51.

Kang, W., Wong, L. C., Shi, S.-H., and Hébert, J. M. (2009). The transition from radial glial to intermediate progenitor cell is inhibited by FGF signaling during corticogenesis. The Journal of neuroscience : the official journal of the Society for Neuroscience, 29(46), 14571-80.

Kanold, P. O., and Luhmann, H. J. (2010). The subplate and early cortical circuits. Annual review of neuroscience, 33, 23-48.

Kato-Negishi, M., Muramoto, K., Kawahara, M., Hosoda, R., Kuroda, Y., and Ichikawa, M. (2003). Bicuculline induces synapse formation on primary cultured accessory olfactory bulb neurons. European Journal of Neuroscience, 18(6), 1343-1352.

Khazipov, R., and Luhmann, H. J. (2006). Early patterns of electrical activity in the developing cerebral cortex of humans and rodents. Trends in neurosciences, 29(7), 414-8.

Knot, H. J., Laher, I., Sobie, E. A., Guatimosim, S., Gomez-, L., Hartmann, H., Song, L.-sheng, et al. (2005). of Calcium Imaging : Cell Physiology to Dye For. Review Literature And Arts Of The Americas, 112-127.

Lappalainen, R. S., Suuronen, R., Skottman, H., and Narkilahti, S. (2010). Similarly derived and cultured hESC lines show variation in their developmental potential towards neuronal cells in long-term culture. Regenerative Medicine, 5(5), 749-762.

Markiewicz, I., Sypecka, J., Domanska-Janik, K., Wyszomirski, T., and Lukomska, B. (2011). Cellular environment directs differentiation of human umbilical cord blood-derived neural stem cells in vitro. The journal of histochemistry and cytochemistry : official journal of the Histochemistry Society, 59(3), 289-301.

Matsubayashi Y., Iwai L., Kawasaki H. (2008) Fluorescent double-labeling with carbocyanine neuronal tracing and immunohistochemistry using a cholesterol-specific detergent digitonin. Journal of Neuroscience, 174(1), 71-81.

Mattia, M., Ferraina, S., and Del Giudice, P. (2010). Dissociated multi-unit activity and local field potentials: a theory inspired analysis of a motor decision task. NeuroImage, 52(3), 812-23.

McMahon, S. S., and McDermott, K. W. (2006). A comparison of cell transplantation and retroviral gene transfection as tools to study lineage and differentiation in the rat spinal cord. Journal of neuroscience methods, 152(1-2), 243-9.

Molecular Probes® Handbook—A Guide to Fluorescent Probes and Labeling Technologies. 11th Edition. Invitrogen. http://www.invitrogen.com/site/us/en/home/References/Molecular-Probes-The-Handbook.html; 09.01.2012.

Morin, F. O., Takamura, Y., and Tamiya, E. (2005). Investigating neuronal activity with planar microelectrode arrays: achievements and new perspectives. Journal of bioscience and bioengineering, 100(2), 131-43.

Nimmerjahn, A., Kirchhoff, F., Kerr, J. N. D., and Helmchen, F. (2004). Sulforhodamine 101 as a specific marker of astroglia in the neocortex in vivo. Nature Methods, 1(1), 1-7.

Opitz, Thoralf, De Lima, A. D., and Voigt, T. (2002). Spontaneous development of synchronous oscillatory activity during maturation of cortical networks in vitro. Journal of neurophysiology, 88(5), 2196-206.

O'Donovan, M. J. (1999). The origin of spontaneous activity in developing networks of the vertebrate nervous system. Current opinion in neurobiology, 9(1), 94-104.

Peinado, A. (2001). Immature Neocortical Neurons Exist as Extensive Syncitial Networks Linked by Dendrodendritic Electrical Connections Immature Neocortical Neurons Exist as Extensive Syncitial Networks Linked by Dendrodendritic Electrical Connections. Journal of Neurophysiology, 85(2), 620-629.

Pettersson, J., Lobov, S., and Novikova, L. N. (2010). Labeling of olfactory ensheathing glial cells with fluorescent tracers for neurotransplantation. Brain research bulletin, 81(1), 125-32.

Pluchino, S., Furlan, R. and Martino, G. (2004). Cell-based remyelinating therapies in multiple sclerosis: evidence from experimental studies. Current opinion in neurology 17, 247-255.

Rajala, K., Hakala, H., Panula, S., Aivio, S., Pihlajamäki, H., Suuronen, R., Hovatta, O., et al. (2007). Testing of nine different xeno-free culture media for human embryonic stem cell cultures. Human reproduction (Oxford, England), 22(5), 1231-8.

Rajala, K., Lindroos, B., Hussein, S. M., Lappalainen, R. S., Pekkanen-Mattila, M., Inzunza, J., Rozell, B., et al. (2010). A defined and xeno-free culture method enabling the establishment of clinical-grade human embryonic, induced pluripotent and adipose stem cells. PloS one, 5(4), e10246.

Rochefort, N. L., Garaschuk, O., Milos, R.-I., Narushima, M., Marandi, N., Pichler, B., Kovalchuk, Y., et al. (2009). Sparsification of neuronal activity in the visual cortex at eye-opening. Proceedings of the National Academy of Sciences of the United States of America, 106(35), 15049-54.

Rouach, N., Segal, M., Koulakoff, a, Giaume, C., and Avignone, E. (2003). Carbenoxolone blockade of neuronal network activity in culture is not mediated by an action on gap junctions. The Journal of physiology, 553(3), 729-45.

Skottman, H. (2010). Derivation and characterization of three new human embryonic stem cell lines in Finland. In vitro cellular and developmental biology. Animal, 46(3-4), 206-9.

Smetters, D., Majewska, a, and Yuste, R. (1999). Detecting action potentials in neuronal populations with calcium imaging. Methods (San Diego, Calif.), 18(2), 215-21.

Sun, C., Warland, D. K., Ballesteros, J. M., van der List, D., and Chalupa, L. M. (2008). Retinal waves in mice lacking the beta2 subunit of the nicotinic acetylcholine receptor. Proceedings of the National Academy of Sciences of the United States of America, 105(36), 13638-43.

Sun, J.-J., and Luhmann, H. J. (2007). Spatio-temporal dynamics of oscillatory network activity in the neonatal mouse cerebral cortex. The European journal of neuroscience, 26(7), 1995-2004.

Takayama, Y., Moriguchi, H., Kotani, K., and Jimbo, Y. (2009). Spontaneous calcium transients in cultured cortical networks during development. IEEE transactions on bio-medical engineering, 56(12), 2949-56.

Voigt, T, Opitz, T., and de Lima, a D. (2001). Synchronous oscillatory activity in immature cortical network is driven by GABAergic preplate neurons. The Journal of neuroscience : the official journal of the Society for Neuroscience, 21(22), 8895-905.

Wagenaar, D. a, Pine, J., and Potter, S. M. (2006). An extremely rich repertoire of bursting patterns during the development of cortical cultures. BMC neuroscience, 7, 11.

Yang, J.-W., Hanganu-Opatz, I. L., Sun, J.-J., and Luhmann, H. J. (2009). Three patterns of oscillatory activity differentially synchronize developing neocortical networks in vivo. The Journal of neuroscience : the official journal of the Society for Neuroscience, 29(28), 9011-25.

Yoshida, R; Iwamoto, A; Nagahama, T. (2001). Calcium imaging for Detection and Estimation of Spike Activities in Apylasia Neurons. ZOOLOGICAL SCIENCE, 18(5), 631-643.

Yuste, R, Nelson, D. a, Rubin, W. W., and Katz, L. C. (1995). Neuronal domains in developing neocortex: mechanisms of coactivation. Neuron, 14(1), 7-17.